NTNU – Trondheim
Norwegian University of
Science and Technology

Characterization of photocatalytic materials used for water treatment

Thorbjørn Salmelid Emdal

Civil and Environmental Engineering
Submission date: June 2015
Supervisor: Stein Wold Østerhus, IVM
Co-supervisor: Cynthia Halle, IVM

Norwegian University of Science and Technology
Department of Hydraulic and Environmental Engineering

Sammendrag

Ettersom trykket på klodens vannkomster øker, er riktig vannbehandling essensielt for å sikre god helse og velferd for befolkningen. Mange kjemiske stoffer fra industri og jordbruk med avrenning til drikkevannskilder eller sårbare resipienter har ikke blitt undersøkt grundig før de har blitt godkjent for bruk.

Mange av disse kjemikalienes påvirkning på miljøet har med tiden blitt ansett som giftige eller bioakkumulerende, og blir derfor ansett som mikroforurensninger. Noen av disse nyoppdagede mikroforurensningene er kjent som *nye miljøgifter* (eng. *emerging contaminants*), men dette er et lite veldefinert begrep (Kümmerer 2011), selv om det opptrer hyppig i vitenskapelig tekst.

Eksempler på slike stoffer er legemidler, fargestoffer, velværeprodukter, vaskemidler og sprøytemidler. Noen av disse stoffene truer med å ødelegge vannkilder og andre akvatiske miljøer.

Dessverre er vanligvis ikke konvensjonelle rensemetoder beregnet for å fjerne mikroforurensninger. Det forskes imidlertid mye på nye renseprosesser kalt avanserte oksidasjonsprosesser (AOP), som viser lovende resultater for fjerning av mikroforurensinger. I denne oppgaven vil en av de mest velkjente, men minst forståtte av AOP-ene bli undersøkt. Den kalles fotokatalyse med bruk av titaniumdioksid (TiO_2) og UV-LED.

Videre er det i forbindelse med oppgaven utført eksperimenter for å finne båndgapet til et stort utvalg materialprøver av modifisert TiO_2. Modifiseringene er gjort gjennom doping med metallioner. Noen av de mest lovende materialene ble testet i en fotoreaktor for å finne radikalproduksjonen sammenlignet med referansematerialet, som er udopet TiO_2.

Resultatene fra båndgapsanalysene viste at de fleste materialene fikk senket båndgapet sammenlignet med referansen på 3.16 eV. Særlig de mangandopede materialene viste stor reduksjon; reduksjonen kom helt ned til 2.89 eV for én av prøvene.

Også målingene fra eksperimentene med radikalproduksjon viste lovende resultater, men ettersom noen av forsøkene ble etterprøvd både én og to ganger viste ingen av dem seg å være reproduserbare. Med andre ord var resultatene fra radikalproduksjonen ugyldige og vanskelig å bruke i diskusjonsdelen.

Dette gjorde dessverre at noe av poenget med masteroppgaven ble borte, da radikalproduksjonen er den vesentligste delen av denne renseprosessen. For prosjektets framtid har riktignok eksperimentene avdekket flere svakheter som kan bidra til bedre oppsett og prosedyrer for videre testing.

Abstract

As the pressure on water bodies throughout the world is increasing, good water quality obtained through water treatment is essential to secure health and welfare of the population. Many chemical compounds used in industry and agriculture with discharge to drinking water sources or vulnerable recipients have not been examined properly before approval.

Many of these chemicals have eventually been considered to be toxic or hostile towards the environment, hence they are called *micro-pollutants*. Some of the newly discovered micro-pollutants are also known as *emerging contaminants*, but this is certainly not a well-defined group of species (Kümmerer 2011), even though it is frequently reported in scientific papers.

Examples of such compounds are pharmaceuticals, dyes, personal care products, soaps and pesticides. Actually, some of them threaten to destroy water sources and other aquatic environments.

Unfortunately, conventional treatment methods are not designed to remove micro-pollutants. However, so-called advanced oxidation processes (AOPs) are up-and-coming water treatment processes that are promising for this matter. In this thesis one of the most well-known, but least understood AOPs are examined. It is called photocatalysis with the use of TiO_2 and UV-LED.

Further, experiments designed to find the bandgap of a large selection of materials of modified TiO_2 have been conducted for this thesis. The modification has been conducted through doping with metal ions. Some of the most promising materials from the bandgap experiments were put in a photoreactor to find the radical production compared to a reference TiO_2 material.

The results from the bandgap analyses showed that most of the materials had decreased bandgap compared to the reference at 3.16 eV. In particular, the manganese-doped TiO_2 materials showed the highest decrease, down to 2.89 eV for one of the samples.

Meanwhile, the radical production experiments had some promising results, but as duplicates and triplicates of the experiments were executed, none of them were reproducible. In other words, the results from the radical production were not valid and could therefore not be used for extensive discussion.

Furthermore, this made large parts of the master thesis pointless, since the radical production is a substantial part of the process. For the future work in the project, the experiments and the revealed weaknesses may, however, contribute to a better setup and procedure for further testing.

Acknowledgements

This master thesis summarize the work I have conducted during the last semester of my five years at the Department of Hydraulic and Environmental Engineering at the Norwegian University of Science and Technology (NTNU), Trondheim, Norway. It has definitely been the hardest topic I have studied these five years. Still, it has been very interesting to be a part of a research field that accommodates hundreds of professors and other researchers all over the world.

My work has been a part of two different projects financed by EU, and for this opportunity I would like to show my appreciation. I would also like to express my gratitude to my supervisors, Professor Stein Wold Østerhus and Associate Professor Cynthia Hallé for motivation, support and guidance throughout the work. KeraNor, represented by Bernt Thorstensen and Ida Johansen, have been a pleasure to co-operate with by providing materials and ideas for the work. Further, PW Circuit in England should be thanked for providing LED discs.

Next, I would like to thank Arne Grostad at the Department for helping me with the design of the photoreactor and for lending me tools whenever needed.

Finally, I thank my wife and friends for motivation and for being supportive the last weeks before the deadline.

Contents

Sammendrag i

Abstract iii

Acknowledgements v

Table of contents viii

List of figures ix

List of tables x

1 Introduction 1

2 Goals and objectives 5

3 Background and literature review 7
- 3.1 Bandgap . . . 8
- 3.2 Radical production theory . . . 9
  - 3.2.1 Superoxide radical ($O_2^{\cdot-}$) and hydrogen peroxide (H_2O_2) . . . 12
  - 3.2.2 The hydroxyl radical ($OH^{\cdot}$) . . . 12
  - 3.2.3 Methods to detect $OH^{\cdot}$ . . . 13
- 3.3 Photocatalysts . . . 14
- 3.4 TiO_2 . . . 15
  - 3.4.1 Physical properties of TiO_2 correlated to photocatalytic activity . . . 16
- 3.5 Modification of TiO_2 . . . 19
  - 3.5.1 Doping . . . 19
  - 3.5.2 Charge carrier traps and recombination centers . . . 20
  - 3.5.3 Metal doping . . . 21
- 3.6 Nitrogen and other non-metal dopants . . . 23
  - 3.6.1 Other modifications of TiO_2 . . . 24
- 3.7 Basic reaction rate theory . . . 25
- 3.8 Support material . . . 27
- 3.9 Bandgap calculations . . . 27
- 3.10 Short summary of the literature review . . . 30

4 Materials and methods 31
- 4.1 pCBA as measurement for radical production . . . 31
- 4.2 Spectrophotometric analysis . . . 31
- 4.3 Photocatalytic reactor . . . 34
  - 4.3.1 Experimental setup and procedure . . . 35
- 4.4 High-Performance Liquid Chromatography (HPLC) . . . 37
  - 4.4.1 Determination of the detection and quantification limits . . . 39
- 4.5 Production methods . . . 41
- 4.6 Analytical methods that should be applied . . . 41

5 Results and discussion **43**
5.1 Bandgap results . . . 43
5.1.1 Analyses of stainless steel samples . . . 44
5.1.2 Analyses of dense alumina samples . . . 46
5.1.3 Analyses of porous alumina samples . . . 48
5.1.4 Reproducibility . . . 49
5.1.5 Sources of error . . . 51
5.1.6 Statistical correlation between dopant properties and bandgap . . . 51
5.2 Radical production results . . . 52
5.2.1 Reproducibility . . . 52
5.2.2 Sources of error . . . 54
5.3 Correlation between bandgap energy and radical production . . . 56
5.4 UV LED light intensity measurement . . . 57
5.5 Quantum yield calculation for reference sample . . . 57

6 Concluding remarks **61**
6.1 Summary and conclusion . . . 61
6.2 Experimental setup . . . 61
6.3 Proposal for future work . . . 61

References **63**

Appendices **69**

Appendix A Calibration curve for HPLC analyses **69**

Appendix B Bandgap results for all samples **70**

Appendix C Data sheets for lab instruments **72**

List of Figures

1 Publication statistics from Scopus 2
2 LED disc used in the experimental part 7
3 Principal drawing of photoexcitation 9
4 Principal drawing of photocatalysis 10
5 Effect of composite anatase-rutile TiO_2 16
6 Principal drawing of TiO_2 doping 19
7 Illustration of the effect of Fe^{3+} doped TiO_2 22
8 Lifetime of charge carriers for doped TiO_2 23
9 Physical parameters influencing photocatalysis 28
10 Example of a bandgap estimation 29
11 Chemical structure of pCBA 32
12 Picture of the 100 mm integrating sphere 33
13 Principal illustration of the integrating sphere 34
14 Kubelka-Munk plot example for bandgap determination 35
15 Picture and illustration of the photoreactor design 36
16 Front panel of the LED control box. 37
17 Calibration curve for pCBA measurements in the HPLC. 38
18 Example output curve for HPLC analysis 39
19 Sketch of the physical structure for the example photocatalyst TiO_2-TiO_2-Fe 0.5M spin. 44
20 Comparison of SS and PA bandgap plot 45
21 Tauc plot with double bandgap 48
22 Reproduction of a spectrophotometric analysis 50
23 Reaction rate for radical production 53
24 Picture of possibly contaminated photoreactor 54
25 Principal illustration of the water surface in reactor 55
26 Light refraction due to angle on water 56
A1 Calibration curve for the HPLC analyses. 69
C1 Data sheet for spectrophotometer with integrating sphere 72
C2 Data sheet for intensity meter with a radiometric sensor, page 1 73
C3 Data sheet for intensity meter with a radiometric sensor, page 2 74

List of Tables

1 Bandgap for several semiconductors 15
2 Regression coefficients for five chemical reactions 18
3 List of photocatalytic reactions 18
4 HPLC output table example 39
5 Detection and quantification limit test for the HPLC 41
6 Bandgap for SS samples 46
7 Bandgap for DA samples 47
8 Bandgap for PA samples 49
9 Bandgap of replicated DA samples 49
10 Treatment efficiency for doped TiO_2 53
11 Results for influence of sampling location 57
12 Light intensity measurements for 375 nm LED disc 58
A1 Data for the calibration curve for HPLC measurements. 69
B1 All bandgap results for PA samples 70
B2 All bandgap for SS samples 71
B3 All bandgaps for DA samples 71

1 Introduction

Most old civilizations are located nearby large water sources. Cairo at the bank of the river Nile, and the ancient Mesopotamia, the cradle of civilizations, lying around the rivers Euphrates and Tigris, are obvious examples. This proves an understanding of the importance of easily available water in large quantities already in the antiquity.

Access to sufficient amounts of fresh water is still a hot topic. In 2013, Egypt threatened to declare a war against Ethiopia because of their huge Renaissance Dam project, making the water discharge in the Blue Nile uncertain for several years. The Blue Nile is, together with the White Nile, the sources of the river Nile that runs through Egypt. The former president of Egypt, Mohamed Morsi, stated that they would defend "each drop of Nile water with our blood if necessary" (Veselinovic 2015). This is only one example of a water induced conflict, and it confirms that water resource management should be a high priority in the years to come, especially on the international scene. A more effective use and also reuse of the water could partly solve some of the serious political issues around the world due to water scarcity.

However, the quality of the fresh water should not be neglected. As populations grow and small villages become towns and cities, water contamination from livestock, farming and from the people themselves increases. The need for more efficient treatment of the water arises accordingly. Boiling and straining the water with cloths has been replaced by advanced mechanical, chemical and biological treatment methods. In spite of increasingly good results in water treatment achieved by the present methods, so-called micro-pollutants are of great concern, and is considered a threat to the water security and ecosystems all over the globe (Bolong et al. 2009; Teh and Mohamed 2011).

According to a huge survey undertaken in various countries in the European Union (EU) by The Gallup Organisation (2009), around 70 % of the participants "thinks that water quality is a serious problem in their country". Not only is the water quality itself a challenge to maintain at a decent level, people's confidence and feeling of security is equally important.

Many micro-pollutants are found in industrial wastewater or in proximity to agriculture. Micro-pollutants in this respect could be industrial solvents, artificial sweeteners, dye, pharmaceuticals, hormones, disinfection by-products (DBPs), pesticides, insecticides, micro-organisms and numerous other micro-pollutants (Richardson and Ternes 2014). Some of the micro-pollutants have a highly unpleasant appearance or odour, and others are accumulating in the ecosystems. The removal of micro-pollutants is particularly important in water reuse systems to avoid accumulation to hazardous levels in the long run.

Micro-pollutants, and also other well known water contaminants (e.g. NOM and

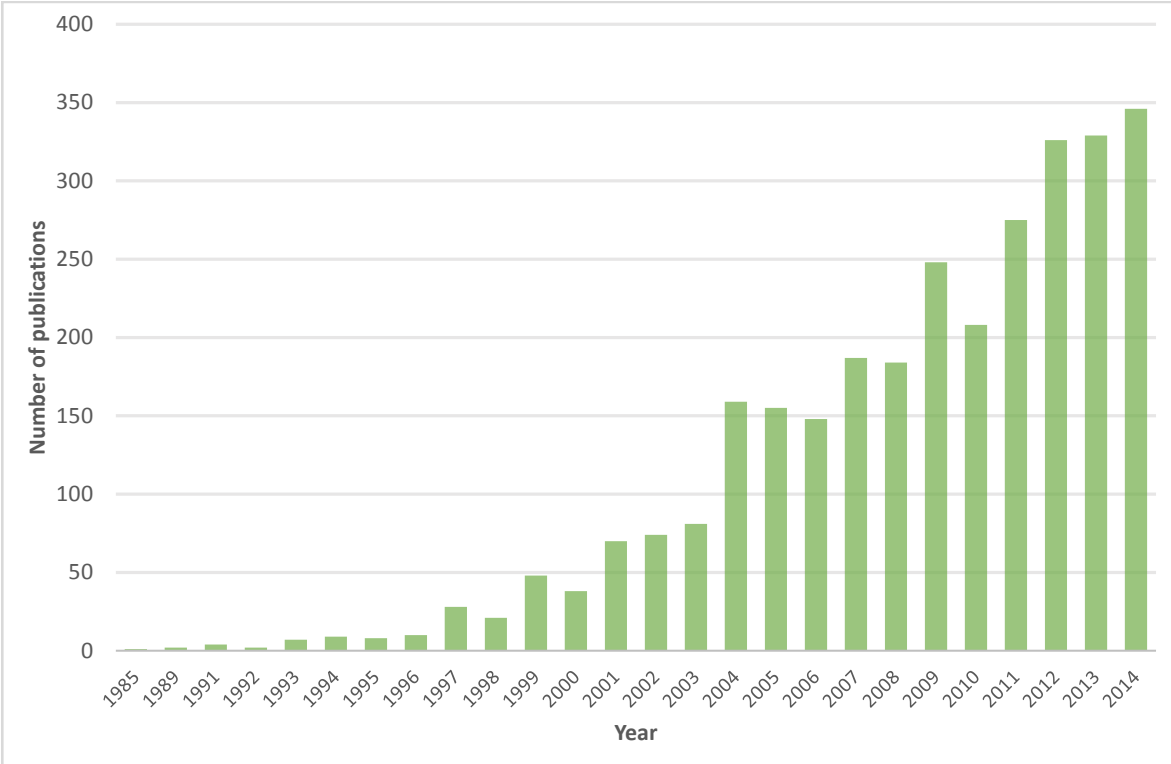

Figure 1 – *Number of publications registered on the keywords "photocatalysis" and "water treatment" in the Scopus database from 1985 to 2014, retrieved from Scopus.com (2015).*

inorganic compounds), could be hard to remove by existing treatment methods due to its chemical stability or low biodegradability. So-called advanced oxidation processes (AOPs) are up-and-coming treatment processes that have shown great results in degradation of many of the mentioned contaminants (Wols and Hofman-Caris 2012; Oller et al. 2011).

UV-Vis/TiO_2 photocatalysis is one of the most interesting processes. It has received tremendous attention the last decades, and the interest is increasing rapidly all over the world, as indicated on figure 1, showing the increasing number of articles and papers published on photocatalysis for use in water treatment the last 30 years. Extensive laboratory work has demonstrated rapid mineralization of organic compounds by the UV/TiO_2 photocatalysis, as well as little accumulation of intermediates (Taborda et al. 2001).

Although general photocatalysis has been researched and developed to a great extent since it first was included in an article title in 1964 (Herrmann 2010), there are quite a few factors that have retained implementation in full-scale water treatment plants (Pichat 2015). Some of those factors will be discussed later.

In this thesis the treatment process photocatalysis with UV/TiO_2, using nothing but

tailor-made LEDs and a stationary catalyst (TiO_2), is examined. No chemical or biological aids are needed in the process, making this particularly interesting as an eco-friendly and inexpensive process. However, it is worth mentioning that this process alone would rarely be sufficient to produce safe drinking water (Lu and Pichat 2013). It is mostly intended as a polishing step to break down organic micropollutants completely, or as a pre-step to turn organic contaminants into a more biodegradable state before other biological treatment (Oller et al. 2011). In addition, it could be used as a disinfection process.

The main idea is to produce hyper-reactive hydroxyl radicals $OH^{\cdot}$ that attack the contaminants in the water, and eventually mineralize them to a non-toxic or otherwise harmless level. Extensive research on how to utilize solar light in the process has been conducted, albeit with varying success (Lu and Pichat 2013). It would certainly be interesting as part of a photovoltaic cell, in addition to self-cleaning materials (Nakaruk et al. 2012).

Unfortunately, visible light (~400-700 nm) accounts for 43 % of the solar light, while UV light (~300-400 nm) accounts for only 4 % (Zou et al. 2001). An unmodified TiO_2 material works only for wavelengths in the ultraviolet spectrum. However, if the photocatalyst could operate inside a wide part of the visible light spectrum, water treatment application, for instance agricultural water treatment in remote areas with little or no electricity could be feasible, particularly if the efficiency of the photocatalysis is increased (Pichat 2015). Hydrogen gas (H_2) could be produced directly from photocatalysis or through more efficient solar cell electricity. As of today, hydrogen gas production is not profitable due to the poor efficiency.

Titanium dioxide (TiO_2) as a photocatalyst

In 1972, Fujishima and Honda discovered that water could be photocatalytically split (i.e. water being both oxidized and reduced at the same time) by illuminating a TiO_2 electrode. This finding initiated a tremendous amount of research to understand and improve the process. Still today, many of the mechanisms involved are poorly understood, and articles are published from several different fields, such as photochemistry, electrochemistry, analytical chemistry, radiochemistry, material chemistry, water chemistry, surface science, electronics and catalysis (Herrmann 2010). This makes the explanation of the different phenomena diverse, quite creative, but unfortunately sometimes inconsistent. For an untrained eye it could be rather confusing and hard to perceive whether the published material is actually veracious or simply qualified guessing.

In this thesis the bandgap energy and radical production potential for different photocatalysts are examined. Especially TiO_2 has proven to be a very applicable material for photocatalysis due to its stability against photocorrosion, low price, and superior photocatalytic activity. TiO_2 also exhibits highly hydrophilic behaviour with a water angle of

0°, making it suitable for industrial applications such as self-cleaning windows and tiles as well as anti-fogging mirrors (Asahi et al. 2014).

For photocatalytic processes in water treatment applications, pushing the bandgap energy down in order to utilize solar light might not appear to be that relevant. With the progress of light emitting diode (LED) technology down to 365 nm (though with decreasing efficiency), even TiO_2 without any doping or other modifications may function in a photocatalytic process. The problem is rather to get the requisite irradiated surface area (Ohtani 2013). However, due to a lower efficiency and higher cost for LEDs with shorter wavelengths, there is still reason to alter the bandgap. This trade-off between a narrowed bandgap, decreased photocatalytic activity and increased LED efficiency for longer wavelengths is interesting, and there is certainly an optimal point where the most efficient combination of catalyst and LED light meet. It would be a big challenge to find this point, but it should still be the goal for this project.

2 Goals and objectives

There are several parties of interest involved in this project, with EU being the project financier. KeraNor, PW Circuits LTD and NTNU are the remaining parties. The primary objective is to optimize an eco-friendly water treatment process to make it economically viable for treating waters with contaminants that are not easily removed by conventional methods, for instance ballast water from cargo ships. The process in the scope of this project is photocatalysis with so-called doped TiO_2 and UV-LED lamps.

KeraNor is a Norwegian research and manufacturing company in the material technology business, whose mission is to develop a photocatalyst preferably with a low bandgap and a high radical production compared to a standard TiO_2 photocatalyst. The photocatalyst should work well with the LED lamps provided by PW Circuits LTD. PW Circuits LTD is mainly a manufacturer of circuit boards, but for this project they contribute with production of new LED technology.

Their wish for this project is to produce LED lamps with as long wavelengths as possible and with high efficiency working with the photocatalysts produced by KeraNor. For the time being, LED lamps with wavelengths that matches standard TiO_2 are both expensive to produce and have a low efficiency.

The Norwegian University of Science and Technology (NTNU) are represented by two professors as well as the MSc candidate writing this thesis. Our goal is mainly to help KeraNor and PW Circuits LTD testing the materials, and give helpful analyses of the results. Hopefully, the results and analyses are of a quality that makes it worthy of publication.

The author has done preliminary testing and screening of materials received from KeraNor and PW Circuits LTD, and will provide some insight in which combination and modification of materials that should be investigated further.

3 Background and literature review

The purpose of this background section is to enlighten the reader in the interdisciplinary and rather complex field of research that photocatalysis with TiO_2 and UV-LED is, but also to build a solid foundation for further discussion of the results attained through the experiments.

In this thesis two main characteristics, bandgap and radical production, of the photocatalytic semiconductor TiO_2 are examined, both through this literature review and through some laboratory experiments. The main attention will be on application in water treatment, but no concrete idea for a reactor design will be presented. The solar cell and hydrogen gas application that accommodates numerous researchers will for the most part be neglected in this literature review.

Extensive research throughout the world to manipulate the bandgap energy has been conducted, often motivated by the desire to utilize solar light (Kumar and Devi 2011), but also due to lower cost and higher efficiency for lamps with longer wavelengths. This has recently become more relevant due to the appearance of the UV-LED technology, making tailor-made LEDs with matching wavelengths for each specific catalyst possible, as for instance the LED disc shown in figure 2.

Alas, the efficiency for LEDs with sub-visible wavelengths decrease rapidly with decreasing wavelengths. A slight red-shift in bandgap energy (i.e. toward longer wavelengths) would yield a significant gain in efficiency. Based on those considerations the bandgap energy is the first characteristic being examined.

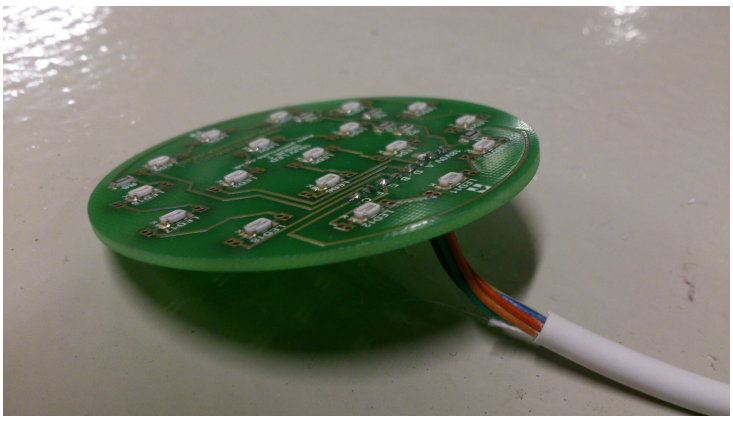

Figure 2 – *The 375 nm LED disc used in the experimental part of the thesis.*

Furthermore, the photocatalytic activity, tightly connected to radical production, is examined, as this is decisive for the efficacy of the water treatment process. There are numerous ways of manipulating the photocatalytic activity; hence, this would be the second characteristic of the photocatalyst.

Shaham-Waldmann and Paz (2013) divides the factors that influence the photocat-

alytic activity into three categories: the physicochemical properties of the photocatalyst, the design parameters for the photoreactor, and operational parameters. The operational parameters, such as pH, temperature, aeration level etc. should be optimized for the specific reactor and reactants, and will not be discussed to a great extent. The physicochemical properties are the ones manipulated through modification of the photocatalyst, and are of the greatest interest. Examples on such catalyst properties are phase, size, energy level structure and surface morphology (Ohtani 2013). Some of them will be discussed in this thesis, but since this field is very complex, and the literature is somewhat incomprehensible and to a certain degree inconsistent, theory that is not understood by the author will not be discussed thoroughly.

Factors restricting the application of photocatalysis
Pichat (2015) suggests that the many obstacles for efficient application of heterogeneous photocatalysis could be summarized in three main principles:

- Shifting the bandgap from the UV spectrum toward the solar spectrum;
- Decreasing the recombination rate of the electrons e^- and holes h^+;
- Increasing the adsorption rate for the contaminants on the photocatalyst surface.

To start with, the basic ideas and concepts of photocatalysis are explained through text and figures, before some of the more complex mechanisms are discussed. Moreover, different modifications to the photocatalyst to alter its restricting properties are investigated.

3.1 Bandgap

A certain amount of photon energy is required to initiate a photocatalytic reaction on a catalyst surface. Electrons (e^-) are excited from the full valence band (VB) to the empty conduction band (CB) in the TiO_2 lattice, leaving a hole (h^+) behind, as shown in figure 3. The electron and hole together are often referred to as an electron-hole pair. Both the electron and the hole are able to react with molecules on the catalyst surface.

The gap between the valence band (VB) and conduction band (CB) is sometimes called the *forbidden gap* owing to the probability close to zero of an electron to exist there by itself, as for all semiconductors. However, the specific amount of photon energy required to excite the electron from the VB to the CB is commonly defined as the *bandgap energy* E_G (Lasa et al. 2005a). The photon energy may come from any light source with the right wavelength and with sufficient energy.

Furthermore, the phenomenon of heterogeneous photocatalysis could be illustrated by a figure similar to figure 4. Electrons are photoexcited from the valence band of the

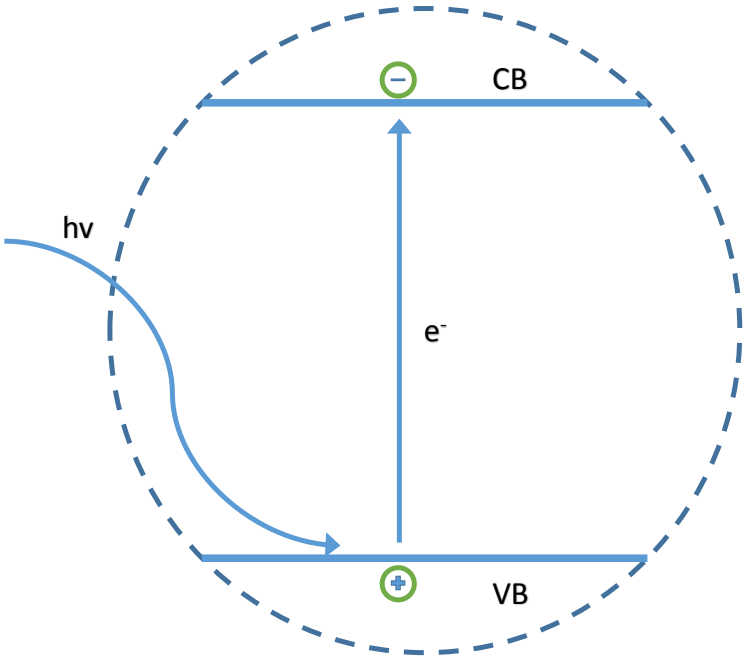

Figure 3 – *Principle drawing of the photoexcitation of a semiconductor (inspired by Linsebigler et al. (1995)).*

TiO_2. Both these free electrons and the holes appearing from the missing electrons may reach the surface of the catalyst where molecules (e.g. water or pollutants) are adsorbed. The electrons reduce the species, while the holes oxidize them. These mechanisms are explained more thoroughly in section 3.2.

Further, adsorbed species can work as electron donors or acceptors. The electron donors are oxidized, and gives away an electron to react with the hole, while the electron acceptors are reduced, and takes a free electron from the CB. This is also further explained in section 3.2.

Unfortunately, visible light carries too little photon energy to overcome the bandgap with pure TiO_2 as the catalyst; hence, light in the ultraviolet (UV) spectrum is necessary. Therefore has the main attention in numerous papers and articles been to modify the photocatalysts to reduce the bandgap (e.g. Nakaruk et al. (2012) and Serpone (2006)).

3.2 Radical production theory

Quantum yield (QY)

An objective magnitude for representation of the efficiency of a photocatalytic process is called the quantum yield (QY), or sometimes quantum efficiency (Herrmann 2010). This is expressed as the ratio between molecules converted per second (reaction rate r) and

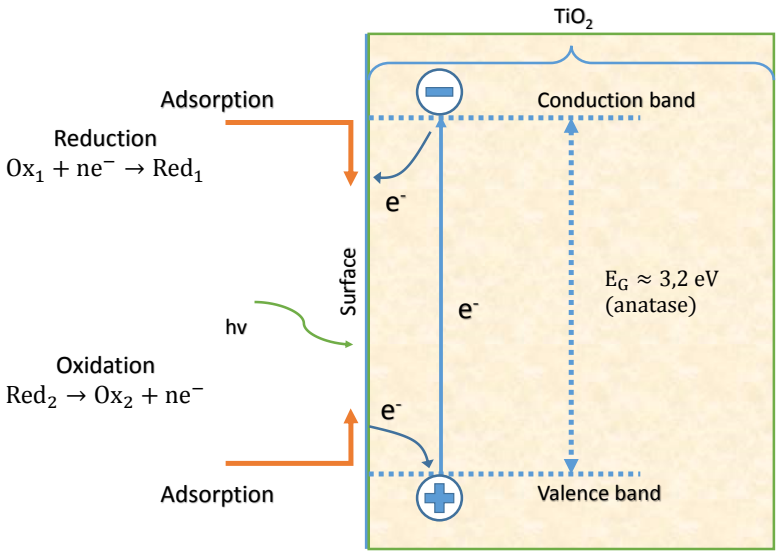

Figure 4 – *Principle drawing of a photocatalytic process, adopted from Herrmann (2010).*

the efficient photonic flux (φ) absorbed by the solid:

$$QY = \frac{r}{\varphi}.$$

In other words, it is a measure for how many molecules that is converted per photon. Further, when the efficient photonic flux is defined as

$$\varphi = \frac{\#\text{ of photons}}{s},$$

and light intensity (i.e. irradiance) is defined as

$$I = \frac{W}{m^2} = \frac{J}{s \cdot m^2},$$

then φ is easily calculated by measuring the light intensity and divide by the energy per photon E and then multiply the surface area:

$$\varphi = \frac{I}{E} \cdot A_{surface}$$

The photon energy E depends solely on the wavelength λ of the irradiation source, as according to the Planck-Einstein relation for a photon

$$E = \frac{h \cdot c}{\lambda} \qquad [eV],$$

where h is the Planck's constant ($h = 6.626 \times 10^{-34}$), and c is the speed of light ($c \approx 300 \times 10^6 \ m/s$). The photon energy E is often referred to as hv due to the relation $v = \frac{c}{\lambda}$. Furthermore, the conversion from electron volt to joule is

$$1 \ J = 6.242 \times 10^{18} \ eV$$
$$\implies 1 \ eV = 1.602 \times 10^{-19} \ J$$

The nature of the reaction rate r is discussed in section 3.7. In fact, the QY magnitude could be a very suitable measurement for the efficiency of a photocatalytic process. Alas, QY is not considered in the majority of papers published on doped TiO_2. However, the QY for heterogeneous photocatalysis with TiO_2 is discussed in section 3.2.2, and a calculation example from the one of the experiments in this thesis is shown in section 5.5.

Radical production equations

When light with hv > E_G is absorbed by the photocatalyst, an electron-hole pair is generated. Radicals are produced when the charge carriers e^- and h^+ reaches the surface of the photocatalyst and reacts with either water, oxygen or hydroxyl groups from a contaminant. Incidentally, contaminants adsorbed to the catalyst surface may react directly with a hole.

Quite naturally, e^- work as a reductant and h^+ as an oxidant, as illustrated in figure 4. Chemically, there are several reactions to consider for heterogeneous photocatalysis (Lasa et al. 2005a):

$$\mathrm{TiO_2} \xrightarrow{\mathrm{hv}} \mathrm{e^- + h^+} \tag{1}$$

$$\mathrm{H_2O} \longrightarrow \mathrm{OH^-_{ad} + H^+} \tag{2}$$

$$\mathrm{h^+ + H_2O_{ad}} \longrightarrow \mathrm{OH^{\cdot}_{ad} + H^+} \tag{3}$$

$$\mathrm{h^+ + OH^-_{ad}} \longrightarrow \mathrm{OH^{\cdot}_{ad}} \tag{4}$$

$$\mathrm{e^- + O_2} \longrightarrow \mathrm{O_2^{\cdot -}} \tag{5}$$

$$\mathrm{O_2^{\cdot -} + H^+} \longrightarrow \mathrm{HO_2^{\cdot}} \tag{6}$$

$$\mathrm{O_2^{\cdot -} + 2\,H^+ + e^-} \longrightarrow \mathrm{H_2O_2} \tag{7}$$

$$\mathrm{H^+ + O_2^{\cdot -} + HO_2^{\cdot}} \longrightarrow \mathrm{H_2O_2 + O_2} \tag{8}$$

$$\mathrm{H_2O_2} \xrightarrow{\mathrm{hv}} \mathrm{2\,OH^{\cdot}} \tag{9}$$

3.2.1 Superoxide radical ($O_2^{\cdot-}$) and hydrogen peroxide (H_2O_2)

Reduction of oxygen molecules are usually the important process in photocatalytic reduction (Nosaka and Nosaka 2013). From eq. (5) an O_2 molecule is reduced by an electron, creating a superoxide radical ($O_2^{\cdot-}$). The superoxide radical is either protonated (eq. 6) or further reduced to form hydrogen peroxide (H_2O_2) (eq. 7), depending on the pH. A one-electron reduction of H_2O_2 forms hydroxyl radicals ($OH^{\cdot}$) (eq. 9).

3.2.2 The hydroxyl radical ($OH^{\cdot}$)

Eq. (3), with a direct oxidation of H_2O to form $OH^{\cdot}$ has actually not been confirmed to occur in photocatalysis, although it is well document in the field of radiation chemistry. In fact, Nosaka and Nosaka (2013) are quite persistent that a reaction like the one in eq. (3) and (4) cannot proceed with a photogenerated hole from the valence band.

Detailed examination with both ultraviolet photoelectron spectroscopy (UPS) (Muryn et al. 1991) and X-ray photoelectron spectroscopy (XPS) (Salvador 2007) proves that water species adsorbed on the TiO_2 surface cannot be directly photooxidized. Instead, the photogenerated holes are assumed trapped at the terminal oxygen ions in the TiO_2 lattice, creating $(O^-)_s$ species (where the subscript s represents the structure). These $(O^-)_s$ species may then be released to oxidize adsorbed molecules.

Furthermore, Henderson (2011) claims that $OH^{\cdot}$ is not always the dominant oxidative species in photocatalysis, oppositely to what most researchers more or less take for granted. Ishibashi et al. (2000) found that the quantum yield of $OH^{\cdot}$ during TiO_2 photocatalysis is approximately 7×10^{-5}, whereas the quantum yield for ordinary photocatalysis is in the magnitude of 10^{-2}. They measured the hole (h^+) generation by iodine ion oxidation to have the quantum yield of 5.7×10^{-2}. Thus, their findings strongly suggest the oxidation by the photogenerated holes to be of a higher magnitude than the hydroxyl radical oxidation for TiO_2 photocatalysis.

Taborda et al. (2001) established that for a photocatalytic reaction with phthalic acid at pH = 4.25, there is a dual hole-radical mechanism where both valence band holes and radicals oxidize the phthalic acid. The direct hole oxidation was made probable to account for the largest part of the quantum yield.

Further, according to Naito et al. (2008) the generation of $OH^{\cdot}$ radicals is very sensitive to the oxygen molecule (O_2) concentration at the surface of the photocatalyst. Consequently, this could indicate that most of the hydroxyl radicals are a result of reduction of O_2 to $O_2^{\cdot-}$, further to H_2O_2 and subsequently ends with the photoreduction of H_2O_2 to hydroxyl radicals (see eq. (5), (7) and (9)).

3.2.3 Methods to detect $OH^{\cdot}$

Measurement of hydroxyl radicals is indeed a difficult task. A common method to get an unambiguous number for the radical production does not seem to exist. However, due to the very short lives of radicals in normal photocatalytic conditions, it is a difficult task to detect radicals directly. Incidentally, several methods for indirect radical detection are developed.

Spin trapping method

A common method to identify and detect the production level of hydroxyl radicals is by the use of a spin trapping reagent (ST). An ST reagent is a slightly unstable compound that reacts covalently (i.e. is "trapped") with free $OH^{\cdot}$ to form a more stable adduct. The adduct is easily detectable by an electron paramagnetic resonance (EPR) spectrometer (often called electron spin resonance (ESR)) (Nosaka and Nosaka 2013; Clément et al. 2005). Consequently, the radical production could in theory be easily estimated. Some of the most popular spin trapping reagents are the nitrone reagents 5,5-dimethyl-1-pyrroline-N-oxide (DMPO) and alpha-phenyl N-tertiary-butyl nitrone (PBN) (Mottley et al. 1986).

However, the spin trapping method should be performed with utmost care, as for instance DMPO could oxidize solely in aerated aqueous solution (Nosaka and Nosaka 2013). Additionaly, if the rate of the hydroxyl radical ($OH^{\cdot}$) generation is much lower than the superoxide ($O_2^{\cdot-}$) production, non-radical products may appear (Finkelstein et al. 1982). Also, photolysis of H_2O_2 to $OH^{\cdot}$ could trap the $OH^{\cdot}$ by excess amounts of DMPO. This could indeed lead to inaccurate radical measurements.

Fluorescence probing method

A fluorescence probing method can utilize more stable reagents than a spin trapping method. This makes the method somewhat more robust. This method has been used frequently in radiation chemistry because of the detectability of the fluorescent products in sensitive detection, especially with the use of terephthalic acid (TA) and coumarine. Hence, it has later been adopted for use in aqueous suspension systems (Ishibashi et al. 2000).

For instance, Yu et al. (2009) used TA as a probe molecule. TA reacts readily with $OH^{\cdot}$, where 2-hydroxyterephthalic acid being the highly fluorescent product detectable at the wavelength of 425 nm. Apparently, the photoluminescence intensity of 2-hydroxyterephthalic acid is proportional to the amount of $OH^{\cdot}$ produced at the TiO_2 surface, and is therefore a good measurement.

Comparison of the methods

Nosaka et al. (2003) compared the two mentioned (amongst other) detection methods for

$OH^{\cdot}$ radical formation in aqueous solutions. The quantum efficiency for the fluorescence method with TA was about 100 times smaller than for the spin trapping method with DMPO. A reasonable explanation suggested could be that somehow both free and adsorbed $OH^{\cdot}$ together with direct valence band hole oxidation are measured with the spin trapping method, while only the free $OH^{\cdot}$ is measured with the other fluorescence probing method. Consequently, the measurements will deviate.

Laser-induced fluorescence

The laser-induced fluorescence method (LIF) was the first method to directly observe the presence of $OH^{\cdot}$ radicals in a TiO_2 photocatalytic system (Murakami et al. 2007). The quantum yield of $OH^{\cdot}$ from the LIF intensity was reported to be 5×10^{-5}, consistent with the findings of Ishibashi et al. (2000) using a fluorescence probe method.

3.3 Photocatalysts

Photocatalysts are materials that, when absorbing photon energy, accelerate the rate of a reaction. It is, by the definition of a catalyst, neither consumed nor chemically changed in the reaction (Lasa et al. 2005c). Semiconductors have particularly suitable properties as photocatalysts due to their electronic structure with an empty void between the top of the full valence band (VB) and the bottom of the empty conduction band (CB) that allows electron-hole pairs to be generated (Kumar and Devi 2011; Linsebigler et al. 1995).

Photocatalysis in water treatment is usually heterogeneous, meaning that the catalyst is in a solid state, while the reactant (e.g. H_2O or O_2) is in liquid or gas phase. The word photocatalytic means that the catalytic reaction is driven by photon energy.

Types of photocatalysts

There are many types of photocatalysts. Metal oxide semiconductors are by far the most suitable for this purpose due to their relatively wide band gap energy, as shown in table 1. Another very useful property is their ability to resist photo corrosion (Fox and Dulay 1993). This is crucial for the photocatalytic activity and lifetime durability.

From table 1 it seems like Fe_2O_3 and CdS are the catalysts requiring the least photon energy. TiO_2 shows the highest *photocatalytic activity*, whereas ZnO follows second of the metal oxides (Ibusuki and Takeuchi 1986).

In fact, the low bandgap energy for many of these materials allows them to absorb light from a wide area inside the visible light spectrum. However, as typical for oxide semiconductors with narrow bandgaps they are photocatalytically inactive due to rapid recombination of the photoinduced electron-hole pair (Dolat et al. 2015).

Table 1 – *Bandgap energies and corresponding radiation wavelength required for the exitation of various semiconductors (Rajeshwar and Ibanez 1997)*

Semiconductor	Bandgap energy (eV)	Wavelength (nm)
TiO_2 (rutile)	3.0	413
TiO_2 (anatase)	3.2	388
ZnO	3.2	388
ZnS	3.6	335
CdS	2.4	516
Fe_2O_3	2.3	539
WO_3	2.8	443

TiO_2 does not only rank highest with regard to activity, it is also inexpensive compared to the rare metal oxides. In addition, TiO_2 is known to be non-toxic, able to oxidize organic compounds (including microorganisms), it is inert both chemically and biologically, and thermally stable (Mandelbaum et al. 1999; Lu and Pichat 2013; Kawahara et al. 2002). Thus, TiO_2 would be the most interesting photocatalyst as subject of research in this thesis.

3.4 TiO_2

There are in general two main principles regarding the design of a TiO_2 photoreactor: fixed-bed or slurry batch reactor (Herrmann 2005). In this thesis slurry TiO_2 is not considered or discussed, although many of the cited authors have used slurry (or powder) in their experiments.

For use in photocatalysts, TiO_2 generally exists in two different crystalline structures: rutile and anatase. The bandgap energy (E_g) of rutile and anatase is $E_g = 3.0$ eV and $E_g = 3.2$ eV, respectively (Bignozzi and Alexander 2011). Despite the slight advantage for rutile regarding the value of the bandgap energy, anatase is much more active than rutile (Tanaka et al. 1991). However, the activity of P-25 (Degussa), a hybrid of anatase and rutile (4/1 % w/w, respectively), often shows higher activity than that of pure anatase. P-25 is therefore a common benchmark photocatalyst (Kawahara et al. 2002).

Nevertheless, the mechanisms governing the increased photoactivity with composite TiO_2 materials like P-25 is not fully understood (Li and Gray 2007). Scanlon et al. (2013) propose a model where the electrons are photoexcited from the rutile VB to CB, and further that the electrons flow to anatase CB, that has a higher electron affinity, as shown in figure 5. This phenomenon facilitates a reduction in the recombination rate, and narrows the bandgap for these composite TiO_2 materials, compared to anatase or rutile.

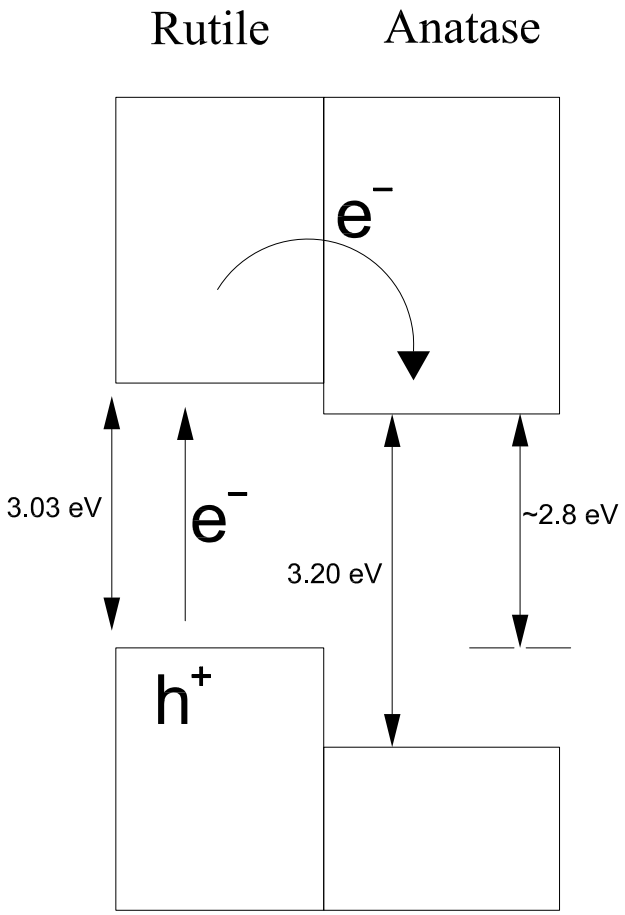

Figure 5 – *Proposed model for the mechanism behind the narrowed bandgap and decreased recombination rate of composite TiO_2 from anatase and rutile. The figure is highly inspired by Scanlon et al. (2013).*

Further, the synthesis of TiO_2 is often performed by the easily controllable sol-gel technique. The product from this technique is mainly amorphous, and in order to get crystalline structure (i.e. rutile or anatase) thermal treatment is required. Many factors, such as temperature, reaction time and the medium, influence the crystallization process. A temperature of 473–493 K was suggested as the optimal (Huang et al. 2000). The particle size in the TiO_2 structure controls the photocatalytic activity to a certain extent. It is therefore important to optimize the synthesis conditions for the TiO_2 materials in order to maximize the photocatalytic output.

3.4.1 Physical properties of TiO_2 correlated to photocatalytic activity

The two most important physical properties regarding its photocatalytic activity are simply the surface area and the number of lattice defects. A large surface area yields adsorption sites, while lattice defects provide electron traps. It is not, however, trivial to find a direct correlation between those properties and the photocatalytic activity. It is

assumed that the different properties are dependent on one another, and also on plenty others (Ohtani 2013).

Anyway, a statistical analysis of the intrinsic effect on the photocatalytic activity of some chosen properties was conducted by Prieto-Mahaney et al. (2009). 35 different TiO_2 powders with five different reactions (a, b, c, d and e) were analyzed. The results are shown in table 2. The reactions are presented in table 3.

The R^2 value represents the squared multiple correlation coefficient. A higher value of R^2 yields a higher reproducibility of the results fitting to a linear combination of properties. The k values represent the partial regression coefficients of the different properties. A positive value means that the photocatalytic activity is increasing with a higher value of the parameter. The higher the value, the higher the increase in activity per change of parameter value. A low or negative value means that the activity is decreasing with a higher value of the parameter. The different subscripts represent:

- BET = specific surface area
- DEF = density of lattice defects
- PPS = primary particle size
- SPS = secondary particle size
- ANA = anatase phase
- RUT = rutile phase

The k values are rather different from reaction to reaction. However, there is a clear trend that k_{ANA} has the biggest influence on the photocatalytic activity. The lower CB edge of rutile is more positive (+0.04 V vs SHE for rutile) compared to the lower CB edge of anatase (-0.20 V vs SHE). When it is known that the potential of $O_2^{\cdot-}/O_2$ is -0.05 V, the slight difference between anatase and rutile potential is assumed to be crucial for the activity for that reaction.

Moreover, the main conclusion from the statistical analysis is that the photocatalytic activity may be estimated quite precisely from the physical properties of the catalyst, at least for the reaction types with the higher R^2 values. For further extensive analysis on the content of table 2, the article by Prieto-Mahaney et al. (2009) is referred to.

Table 2 – *Squared multiple correlation coefficient (R^2) and partial regression coefficients (k) for five given chemical reactions (Prieto-Mahaney et al. 2009).*

Coefficient	a	b	c	d	e
R^2	0.86	0.52	0.58	0.60	0.85
k_{BET}	−0.01	0.43	−0.09	0.13	0.19
k_{DEF}	−0.15	−0.25	0.19	0.43	0.32
k_{PPS}	0.12	−0.20	−0.18	−0.20	−0.52
k_{SPS}	0.57	0.08	−0.20	−0.04	−0.07
k_{RUT}	0.14	0.28	0.11	−0.06	0.02
k_{ANA}	0.04	0.40	0.57	0.55	0.63

Table 3 – *List of photocatalytic reactions for evaluation of activities, simplified from Prieto-Mahaney et al. (2009).*

Entry	Stoichiometry
a	$4\,Ag^+ + 2\,H_2O \longrightarrow 4\,Ag + O_2 + 4\,H^+$
b	$CH_3OH \longrightarrow HCHO + H_2$
c	$CH_3COOH + 2\,O_2 \longrightarrow 2\,CO_2 + 2\,H_2O$
d	$CH_3CHO + \frac{5}{2}O_2 \longrightarrow 2\,CO_2 + 2\,H_2O$
e	$\text{L}-\text{lysine} \longrightarrow \text{L}-\text{Pipecolonicacid} + NH_3$

3.5 Modification of TiO_2

3.5.1 Doping

In general terms, doping means incorporation of a strange ion or atom element into the photocatalyst. However, the term ”doping” has no unambiguous definition in the literature. ”Doping” is used regardless of whether it is the lattice structure or the surface being modified. Often the authors avoid discussion about the actual location of the dopant atoms or ions in the photocatalyst, although it is of utmost importance for the photocatalytic properties (Ohtani 2013).

As mentioned earlier, the main purpose of doping TiO_2 has historically been to utilize light from the visible light spectrum. The general way of doing this is to narrow the bandgap. A principal drawing of this is shown in figure 6. The idea is to find a dopant that has a VB and CB slightly above the VB and CB of the TiO_2, but with a smaller bandgap. When an electron is excited in the dopant, it will go from the VB to the CB, as usual. Subsequently, due to the more positive CB of the TiO_2, the electron will be attracted and ”jump over”. This way the bandgap of the TiO_2 has been narrowed.

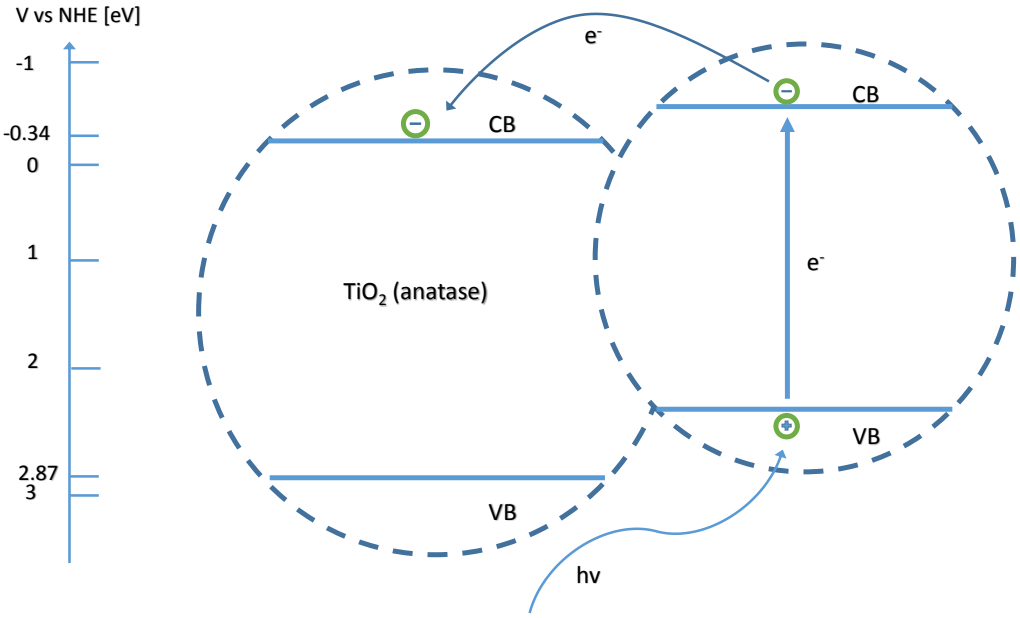

Figure 6 – *Principle drawing of doping of anatase TiO_2 where the narrowing of bandgap happens due to the different energy levels of the conduction bands, inspired by Kumar and Devi (2011).*

Actually, it is claimed that any photocatalyst with poor activity under *visible light irradiation* is enhanced by adding a metal or non-metal as a dopant (Ohtani 2013). Although a lot of effort has been put into development of visible light driven photocatalysts, but enhancement of the *photocatalytic activity* has been somewhat neglected, and most

researchers have failed to prove that doping leads to visible-light induced photocatalysis. In fact, a common methodology to distinguish between actual photocatalytic improvement and simply random side effects of the dopants or the chemicals used to measure the activity has not appeared in this field (Ohtani 2013).

However, the main challenge with doping is the increased recombination rate. According to Herrmann (2010) traditional doping with cations is *always* unfavourable, and sometimes even "catastrophic" for photocatalysis. The reason is that doping with cations creates recombination centres.

3.5.2 Charge carrier traps and recombination centers

To make photocatalytic charge transfer more efficient, decreasing the recombination rate is an important measure (Linsebigler et al. 1995). Recombination is a phenomenon where the photoinduced electron in the conduction band reacts with a corresponding hole in the valence band and heat is released; thus, the photon energy used to excite the electron has gone to waste (Dong et al. 2015).

Electrons cannot exist by itself within the forbidden gap in the bulk, as mentioned in section 3.1. On the contrary, there are many electron energy states at the surface of the semiconductor where the charge carriers may be trapped. Di Valentin and Selloni (2011) show that the trapping energy is larger at the surface compared to the bulk of the TiO_2, suggesting that a travel toward the surface is favourable for the charge carriers.

According to Ohtani (2013) it is shown many times, often with the use of electron paramagnetic resonance (EPR), that ${Ti_4}^+$ is reduced to ${Ti_3}^+$ in certain locations in the lattice of the TiO_2 during photocatalysis. In other words, the electrons are rapidly trapped, making it possible for the holes to react with surface species or with oxygen in the lattice without recombining.

When an electron acceptor, sometimes called a scavenger, such as O_2 is adsorbed on the surface, the charge should be released from the trapped state for the photocatalysis to function.

Addition of transition metal ions to the TiO_2 structure has proven to enhance the photoreactivity of the catalyst by acting as traps for either electrons or holes, depending on the metal ion being electron acceptor or donor (Choi et al. 1994; Pichat 2015), corresponding to an n-dopant and p-dopant. Trapping of either one of the charge carriers prevents it from recombining with the counter carrier. The result is therefore an increase in lifetime of the electron-hole pairs so it reaches the surface of the photocatalyst before recombination.

Further, electron scavengers increase lifetime of photoinduced holes. Molinari et al. (2015) examined the influence of carbonate (${HCO_3}^-$) as an electron scavenger in TiO_2

photocatalysis. The reduction product of HCO_3^- is the formate radical $^{\bullet}CO_2^-$, which is easily detectable. A linear relation between the carbonate concentration and the amount of $OH^{\cdot}$ in the water, indicates that the lifetime of holes is strongly dependent on an electron scavenger.

3.5.3 Metal doping

Doping with transition metals increases the level of Ti_3^+ ions in the TiO_2 lattice. The Ti_3^+ ions causes an increased formation of oxygen defects, leading to a more efficient adsorption of oxygen molecules at the catalyst surface (Kumar and Devi 2011).

Estimation of the photocatalytic effect of doped TiO_2 is dependent on dopant concentration, energy level of dopants within the catalyst lattice, distribution of dopant, light intensity, electron donor concentrations and the d electronic configuration (Choi et al. 1994).

Manganese doping

Deng et al. (2011) conducted experiments with addition of manganese (Mn) to TiO_2 nano-powder produced using a sol-gel method. Their experiments showed that the photocatalytic degradation of methylene blue (MB) was significantly better with the Mn doped TiO_2 than with the pure TiO_2 in visible light. The research showed that a Mn content of 0.2 at% was optimal, whereas concentrations of Mn below and above yielded a poorer degradation rate (i.e. lower photocatalytic activity). The research did, however, not show anything about the quantum efficiency compared to TiO_2 in UV light.

Iron doping

According to (Choi et al. 1994) dopants with closed shell electronic structure, such as Li^+, Mg^{2+}, Al^{3+}, Zn^{2+}, Ga^{3+}, Zr^{4+}, Sn^{5+}, and Ta^{5+} had little or no positive effect on the photocatalytic activity. Contrarily, Fe^{3+} doping showed enhanced performance compared to undoped TiO_2. The explanation is quite simply that Fe^{3+} may trap both electrons and holes, and achieve an oxidation state of Fe^{2+} and Fe^{4+}, respectively. Fe^{2+} and Fe^{4+} are, according to crystal theory, unstable compared to Fe^{3+}, and will seek to re-establish its stable state by detrapping the charge carriers, as illustrated in figure 7.
Next, if the iron doping is not too extensive, the charge carriers will be able to react with oxygen and surface hydroxyl groups on the catalyst surface, instead of with each other (Yu et al. 2009). Thus, finding the optimal dopant concentration is vital for suppressing the recombination rate.

Chromium and molybdenum doping

Wilke and Breuer (1999) conducted experiments with Cr^{3+} and Mo^{5+} doped TiO_2 photo-

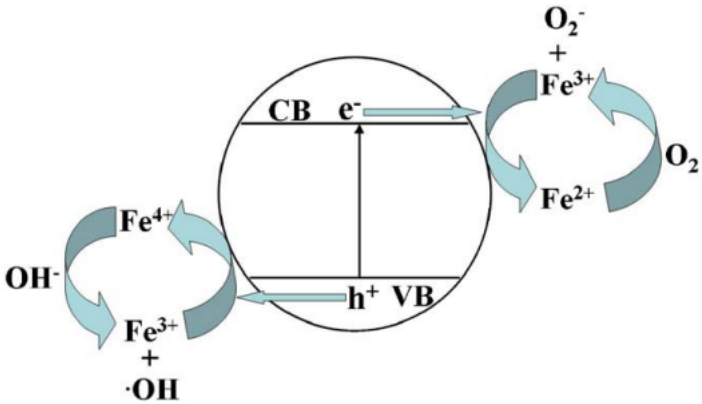

Figure 7 – *Principal illustration of the Fe^{3+} acting as a mediator of interfacial charge transfer. The Fe^{3+} works as both electron donor and acceptor, and could possibly decrease the recombination rate. The figure is retrieved from Yu et al. (2009).*

catalysts produced with the sol-gel method. The purpose of the experiments was to reveal the effect of Cr^{3+} and Mo^{5+} on the lifetime of the electron-hole pairs generated in the photocatalytic reaction, and also find the difference in surface adsorption of Rhodamine B (dye) compared to undoped TiO_2. It was found that both chromium and molybdenum decreased the lifetime of the electron-hole pairs significantly already at very low concentrations, as shown in figure 8. A possible explanation for the decreased lifetime could be trapping of both the charge carriers, obstructing them from reaching the surface, and instead recombine with the opposite charge carrier. Thus, the dopant could be deemed a recombination center.

However, Mo^{5+} doped TiO_2 showed great adsorption attraction towards Rhodamine B compared to undoped TiO_2. It is suggested a strong electrostatic interaction between the strongly positively charged Mo^{5+} and the electron-rich center of the dye molecule, enhancing the adsorption rate significantly. The same effect was absent with the Cr^{3+} doped TiO_2.

The sum of charge carrier lifetime and adsorption showed a clear correlation with the photocatalytic activity of the photocatalyst (Wilke and Breuer 1999), albeit none of the doped catalysts in their study showed better results for photocatalytic activity compared to undoped TiO_2.

Zinc doping

Zhiyong et al. (2007) doped TiO_2 with zinc (Zn) to form $ZnSO_4{-}TiO_2$ Raschig Rings (RR). Degradation of Orange II was found to be higher with the doped catalyst than with the commercial Degussa P25 under a broad-spectrum irradiation with a peak at $\lambda = 366$. The short suggestion for why this enhancement could take place was that the Zn-atoms acted as electron acceptors, while the TiO_2 lattice worked as an electron donor.

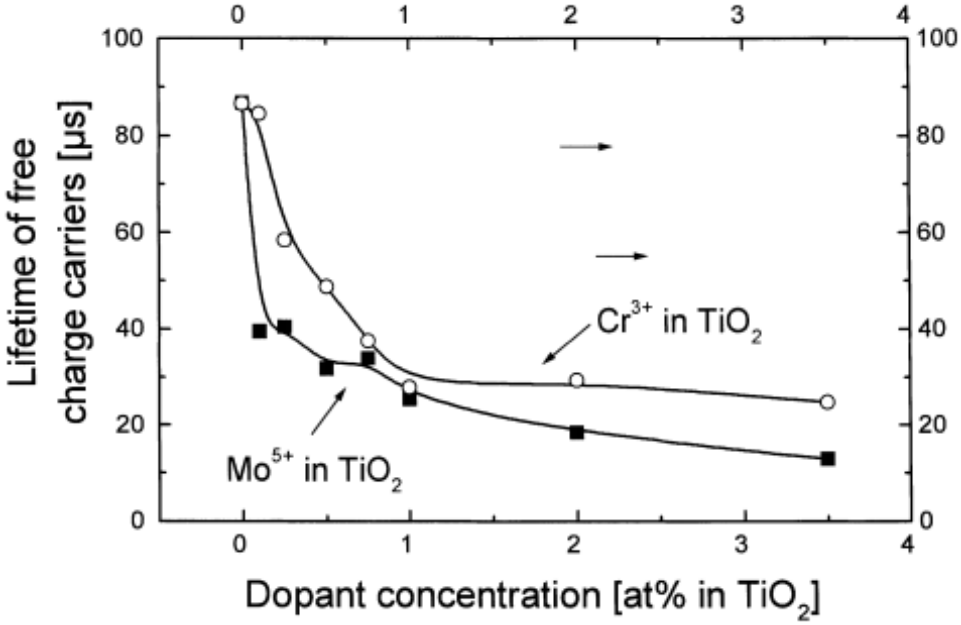

Figure 8 – *Lifetime of the charge carriers e^- and h^+ in microseconds as a function of dopant concentration with chromium and molybdenum (Wilke and Breuer 1999).*

This suggestion was supported by findings in an x-ray photoelectron microscopy (XPS) analysis of the tested samples.

Scandium doping

Scandium has about the same ion radius as titanium, and scandium oxide are therefore expected to form solid solution with TiO_2 when TiO_2 is doped with scandium. The scandium oxide has been reported to *increase* the bandgap of anatase, as well as increasing the particle size (Hirano et al. 2005).

Further, Cavalheiro et al. (2008) observed that a low concentration of scandium in the TiO_2 structure increased the number of defects that in turn reduced the cell volume due to the reduction of the crystallinity. However, a further increase in the scandium concentration up to 5 mol % actually enhanced photocatalytic activity, and reduced the bandgap. It was suggested that additional negative charge carriers were generated due to the doping.

3.6 Nitrogen and other non-metal dopants

Asahi et al. (2001) were the first to discover that non-metal doping (with nitrogen) of titania could change the absorption spectre toward visible light and alter the photocatalytic activity. Anionic doping with nitrogen is extensively explored the last decade, especially with hydrogen production as the goal. The main issue in this regard is to get hold of

electron donors that can occupy the photoinduced holes to avoid recombination and reversion of H_2 to water. Some researchers have suggested the use of scavengers such as carbonate salts or even wastewater to fill the holes, and this has given higher quantum efficiency for some scavenger species such as methanol and ethanol (Ni et al. 2007).

Dolat et al. (2015) conducted experiments on nitrogen-doped rutile TiO_2, metal-doped rutile TiO_2, and metal-nitrogen-co-doped rutile TiO_2 (Me,N-TiO_2/R). The two former showed some photocatalytic activity, though with poor performance. The Me,N-TiO_2/R showed significantly improved performance both under visible and UV light irradiation. The nitrogen and the presence of $Ti_3{}^+$ ions in the TiO_2 structure reduced the bandgap.

However, the metal used in the co-doping was of great importance. It was concluded that the proper amount and form of the metal on the TiO_2 surface greatly enhanced the charge separation. In the study it was further concluded that nickel (Ni) yielded a dramatic increase in photocatalytic activity even under UV light irradiation, and the results were slightly better than for commercial Degussa P25 in UV light. These results show that co-doping of TiO_2 with non-metals and metals could in fact decrease the bandgap without increasing the recombination rate.

Additionally, the chemical reaction used to test the activity was degradation of acetic acid to CO_2 - a method not observed elsewhere by the author.

Further, doping with sulphur, fluorine, boron and other non-metal species are also found in the literature. By reviewing the photocatalytic activity of several studies with different non-metal dopants, Asahi et al. (2014) claims that nitrogen still are the best of these. Furthermore, it is claimed that the origin of the visible-light activated photocatalysis of N-doped TiO_2 is very much debatable, and not at all fully understood. Still, a lot of research has been carried out based on assumptions of possible reaction mechanisms that is overwhelmingly complex for the author of this thesis.

3.6.1 Other modifications of TiO_2

In a review article by Kumar and Devi (2011) several of the most common TiO_2 modification principals were listed. The list includes: coupling TiO_2 with a narrow bandgap semiconductor, metal or non-metal ion doping, co-doping with other foreign ions (as described briefly in sec.3.6), surface sensitization by organic dyes or metal complexes, surface fluorination, and noble metal deposition. None of these modifications will be discussed here.

The literature on surface sensitization describes physical and chemical mechanisms that tend to be of a particularly complex nature, and will certainly not be discussed in this thesis.

Pushing the bandgap of TiO_2 towards longer wavelengths has been a subject of research

for decades. Due to the arrival of high energy LEDs down to as low as 365 nm, Izadifard et al. (2013) suggest that, for water treatment applications, attention should shift from pushing the bandgap energy to actual performance of the catalyst in form of radical production.

One of the most important properties of a photocatalyst is the surface area accessible for the molecules that are subject of degradation. With the coming of more advanced nanotechnology, this has become a serious field of research the last few years. Graphene is a diverse material that could be used for modification of TiO_2.

Graphene modification of TiO_2

One of the most up-and-coming materials at the present time is graphene. The role of graphene as a photocatalytic modifier is extensively researched. According to a review article by Upadhyay et al. (2014), graphene can:

- reduce recombination due to its electron accepting nature;
- increase the organic pollutant adsorption;
- narrow the bandgap;
- increase the surface area;
- increase the mechanical strength of the adsorbent;
- damage the cell membranes of microorganisms due to its sharp edges.

Although these properties of graphene seem promising, the technology for synthesis of high quality graphene is not fully developed, and full control of the defects and layer structures is not yet achieved. According to the same review article, the hybrid of TiO_2 and graphene may offer selectivity towards specific ions and molecules. These findings are interesting, but one of the main issues is apparently the waste disposal and recycling of the expired composite photocatalyst, making it unsuited for water treatment applications.

3.7 Basic reaction rate theory

The fundamental principal behind the reaction rate of a photocatalytic process could be represented like this (Ohtani 2013):

$$\text{Rate} = \text{Irradiance} \times \text{photoabsorption efficiency} \times \text{quantum efficiency}$$

Irradiance represents the photon flux from the light source, photoadsorption efficiency represents the number of active sites in the system, whereas quantum efficiency represents how many molecules of reactant that is converted per photon absorbed by the catalyst.

Further, the Langmuir-Hinshelwood (L-H) kinetic expression is commonly used to describe the kinetics of heterogeneous catalytic processes (Kumar et al. 2008). The expression is given by

$$r = -\frac{dC}{dt} = \frac{kSKC}{1 + KC} \tag{10}$$

where K is an equilibrium constant of adsorption, S is the limiting amount of surface adsorption, k is the true reaction constant for the surface-adsorbed reaction between the reactant and e^-/h^+. C is the concentration of the reactant in the liquid bulk at equilibrium.

According to Herrmann (2010) the true rate constant k for the photocatalytic activity is dependent only on the radiant flux (e.g. light intensity); notably, k being dependent on the reactant concentration is a common misconception among researchers. However, the L-H equation as it is stated in eq. (10) is valid for monomolecular reactions only. Another set of parameters is necessary if two or more molecules participate in the reaction. In the experiments in this thesis several molecules are gradually present, and it is therefore not a true monomolecular reaction.

Further, Herrmann (2010) states that there are five physical parameters governing the photocatalytic activity: mass of catalyst, wavelength, initial concentration of reactant, temperature, and radiant flux. As shown in figure 9 A, B and C, both mass, wavelength and initial concentration are parameters that reaches an optimal point before the curve for r flattens to a constant value plateau.

For temperatures between 20 and 80 °C r would be more or less constant, but for colder or warmer temperatures, the reaction rate in figure 9 D seems to be somewhat decreased. This is due to K's dependence on temperature, as according to thermodynamic laws.

Catalyst mass, m

The mass m of the catalyst determines the number of active sites for the photons to be absorbed. Let n_{as} be the number of active sites, d_s the areal density of sites, and A_s the specific area of the catalyst, then we have the relation

$$n_{as} = m \cdot d_s \cdot A_s.$$

In general, leaving the other parameters constant, an increase in m from zero up to a certain treshold m_{opt}, would lead to a linear relation

$$r = f(m \leq m_{opt}) \propto m$$

followed by a plateau with no further elevation of the curve for higher values of m

$$r = f(m > m_{opt}) = constant,$$

as showed in figure 9 A. The linear part of the curve proves a fully true photocatalytic reaction behaviour, because the reaction rate increases proportionally with the area. When the curve flattens it is probably a sign of insufficient illumination of the photocatalyst.

This type of curve should be determined in the design of a photocatalytic reactor to avoid using too much catalyst mass, and to ensure that all the catalyst is irradiated by the light source (Herrmann 2010).

Wavelength, λ

The wavelength λ is inversely proportional to the photon energy hv

$$\lambda \propto \frac{1}{hv}.$$

As seen in figure 9 B, the reaction rate r is constant for all wavelength up to the wavelength corresponding to the bandgap energy level E_G. For any wavelengths greater than E_G, no reaction will initiate. Thus, the reaction is either going or not going, depending on the photon energy to be either higher or lower than E_G, respectively.

3.8 Support material

For immobilized TiO_2 a support material is convenient to anchor the catalyst in a reactor, either through physical surface forces or chemical bonds. The support material could represent the walls, lamellas or other parts of a reactor reachable by light. Relevant support materials with references to real experiments are listed in Lasa et al. (2005b). The list consist of: activated carbon, fiber optic cables, several different glass materials, zeolites, silica gel, stainless steel, and teflon.

The support materials provided for the experiments in this thesis are dense alumina, porous alumina and stainless steel.

3.9 Bandgap calculations

The bandgap energy E_G for diffuse reflectance is commonly found using the Kubelka-Munk (K-M) method (Yu et al. 2009). According to López and Gómez (2012) the optical methods for finding the bandgap of a semiconductor (e.g. TiO_2) could be justified due to the independence of temperature and surface uncertainties. However, in the same article it is claimed that inconsistencies appears frequently in the literature regarding calculations

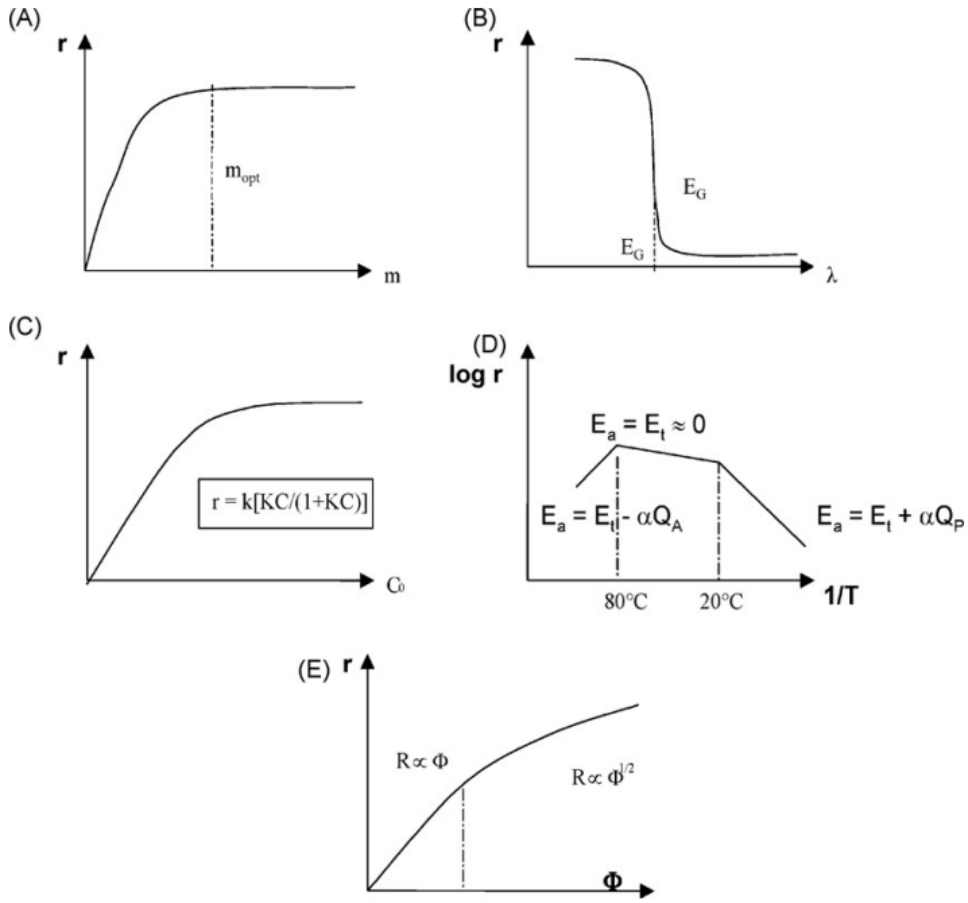

Figure 9 – *Kinetic influence of the parameters responsible for the photocatalytic activity, reaction rate, r; (A) mass of catalyst m; (B) wavelength λ; (C) initial concentration c of reactant; (D) temperature T; (E) radiant flux Φ. (Adopted from Herrmann (2010)).*

of the bandgap energy. The confusion seems to arise when it is not obvious whether the transition is direct or indirect. In addition, there are several calculation methods applied uncritically without being justified whatsoever.

In immediate danger of falling into the same trap in this discussion, the bandgap energy is estimated by plotting $(\mathrm{F(R\infty)} \cdot \mathrm{hv})^{0,5}$ against the photon energy (hv) in accordance with a Tauc plot (Tauc et al. 1966). $\mathrm{F(R\infty)}$ is the absorption coefficient as a function of the reflectance R. The relation between R and $F(R\infty)$ is

$$F(R\infty) = \frac{(1-R)^2}{2R}.$$

The wavelength λ is inversely proportional to the photon energy hv, as described in section 3.2. The photon energy is measured in electron volt (eV), as follows

$$hv \approx \frac{1240}{\lambda}.$$

For semiconductors like the ones listed in table 1, a sudden climb in light absorption with decreasing wavelength is observed. The sudden alteration of the curve is consistent for materials able to absorb photons. The intercept between the tangent of this steep (and linear) part of the Kubelka-Munk curve and the x-axis gives an estimate of the bandgap, as shown in figure 10.

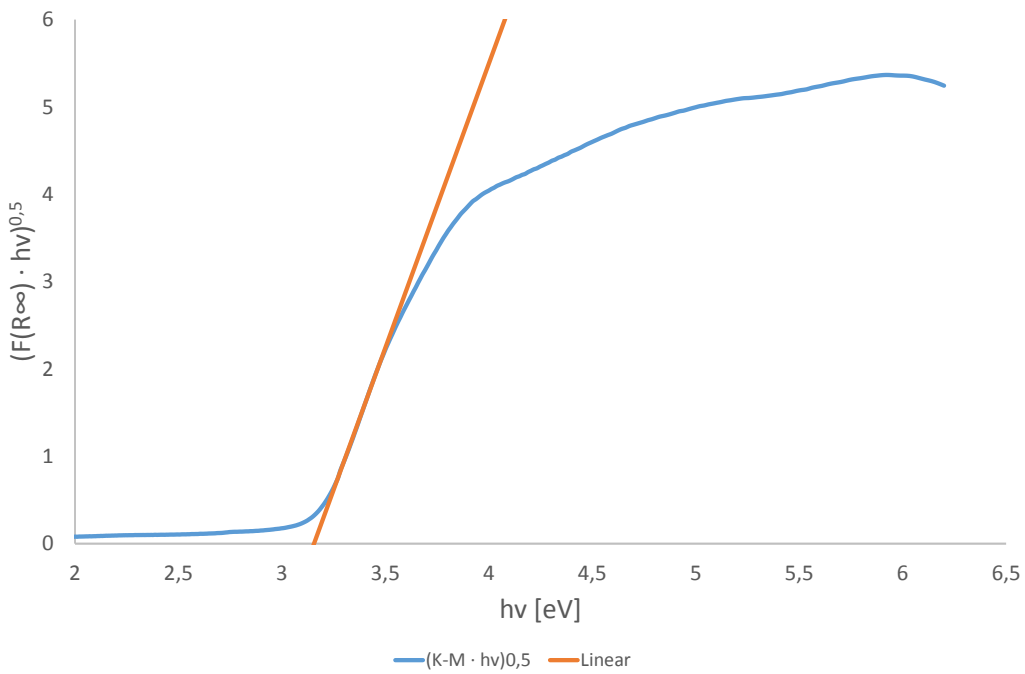

Figure 10 – *Example of a Tauc plot where the linear extrapolation of the steepest part of the curve intercepts with the x-axis and gives the bandgap. In this case the bandgap is ~3.1 eV.*

3.10 Short summary of the literature review

The chapter started with some fundamental theory and description of concepts. Then papers, articles and text books written by different researchers with very diverse backgrounds were discussed.

As only a tiny fraction of the vast amount of literature has been reviewed in this thesis, it seems like doping of TiO_2 will not yield better quantum efficiency than undoped TiO_2 in most cases. Apparently, doping is a trade-off between narrowing the bandgap and loss of quantum yield. Herrmann (2010) clearly states that at least *cationic* doping is always affecting the quantum yield negatively.

On the contrary, anion doping with nitrogen is seemingly a better options than the more traditional metal-doping. A recent study by Dolat et al. (2015) showed both increased photocatalytic activity and narrowed bandgap with co-doping of N and Ni in UV light. The benchmark sample they used was P-25 Degussa.

However, it is a tough challenge to compare different studies due to the different approaches and methods. In addition, it seems like methods often are constructed to produce results that look good. A very common example is radical production (or photocatalytic activity) measurements from doped TiO_2 compared to undoped TiO_2, conducted in visible light. Obviously, doped TiO_2, which usually has a narrowed bandgap compared to undoped TiO_2, will show higher photocatalytic activity when the light has a photon energy lower than the bandgap of the undoped TiO_2, but higher than the doped TiO_2 bandgap.

Because there does not seem to exist a consensus amongst the TiO_2 researchers on how to perform commensurable studies, extensive discussion on the effect of different dopants have not been included here.

4 Materials and methods

Two analytical methods were used in the laboratory work for this thesis. First, UV-visible/diffuse reflectance spectrophotometer (UV-vis/DR) was employed to estimate the bandgap energy. A good picture of the bandgap energy for the different catalysts was obtained through the UV-vis/DR analyses.

Second, high performance liquid chromatography (HPLC) was employed to analyze water samples taken from the photocatalytic reactor.

4.1 pCBA as measurement for radical production

p-chlorobenzoic acid (pCBA) was chosen as the chemical compound degraded for measurement of radical production in the photocatalysis. This choice was made based on experience from the supervisors. pCBA is an important intermediate species in several industries, such as pesticide, dye and pharmaceutics, and is known to be bio-recalcitrant. Furthermore, it accumulates in the environment as an intermediate product from the biodegradation of chlorinated aromatics (Han et al. 2004).

According to Jenks (2013), benzoic acid and various derivatives of it have been extensively studied under photocatalytic degradation conditions. Moreover, the product species from the photocatalysis are reported to be salicylic acid, other hydroxylated benzoic acids and phenols (though in trace amounts). Thus, there is most likely more than one product from the degradation of pCBA. Consequently, this makes degradation of pCBA unsuited for estimating absolute radical production.

However, pCBA is a very stable compound in aqueous solution due to its aromatic ring, as shown in figure 11. It is, however, degradable by hydroxyl radicals; thus, pCBA should be ideal for photocatalytic experiments. Next, if it is used to compare the efficiency between a selection of catalysts, it seems like a good choice of species.

Anyway, the HPLC showed a stable and performance for the measurement of pCBA, as discussed in section 4.4.

However, in order to get a good indication of the activity of a photocatalyst, more than one chemical compound should be analyzed. Several compounds with differing reaction pattern and reaction rates were examined by Prieto-Mahaney et al. (2009) (ref. section 3.4.1). Their experiments shows the importance of selecting the right chemical species for the purpose.

4.2 Spectrophotometric analysis

A UV-visible spectrophotometer can measure diffuse reflectance of the photocatalyst for a wide wavelength spectrum, and further be used for estimating the bandgap energy. The

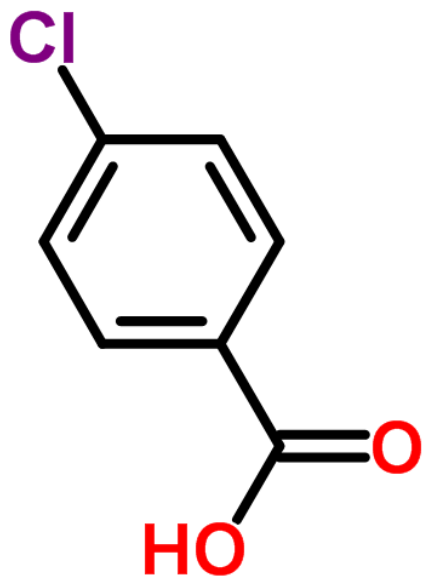

Figure 11 – *Structure of the p-chlorobenzoic acid (pCBA) compound used to indirectly measure radical production, retrieved from ChemSpider.com (2015).*

spectrophotometer used in the current experiments was a PerkinElmer UV/VIS Spectrometer Lambda 650 with a 100 mm Integrating Sphere attachment.

First, the equipment was calibrated with a Spectralon standard. The square-shaped material samples had a surface area of 5x5 cm^2, while the circular samples had a diameter of ~ 76-77 mm, corresponding to an area of ~ 46 cm^2. The sample was put in a window on the wall of the integrating sphere. A picture and some explanatory text is provided in figure 12. In addition a principal sketch is shown in figure 13.

Thereafter, the sample was irradiated by light with wavelengths from 200 to 900 nm, with an incremental step of 1 nm. The diffuse reflectance for each wavelength was measured by a sensor inside the integrating sphere. The raw data output to the computer software was reflectance R as a function of the wavelength λ. R was converted to the Kulbelka-Munk function, as described in section 3.9:

$$KM = (\mathrm{F(R\infty)} \cdot \mathrm{hv})^{0,5}$$

The wavelength (λ) was converted to photon energy (hv), also as described in section 3.9:

$$hv \approx \frac{1240}{\lambda}.$$

To find the steepest part of the curve, the curve was differentiated in MS Excel for every step x_i of the KM function. Since the steps on the x-axis are nearly the same, the

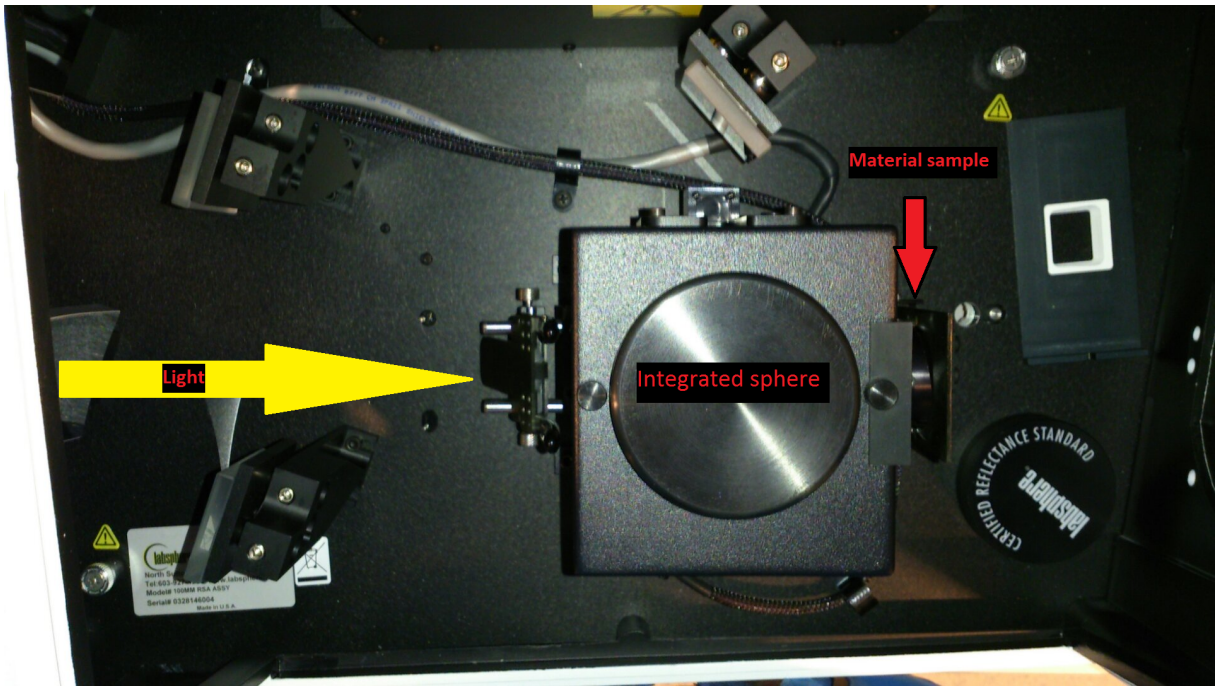

Figure 12 – *Picture of the PerkinElmer 100 mm integrating sphere. The light comes from the left and hits the material sample on the right side of the integrating sphere. Then some of the light is absorbed by the sample, and the rest is reflected inside the sphere until it hits the photodetector.*

differentiation is simplified to be

$$\frac{d(KM_i)}{dx} \approx KM_i - KM_{i-1}.$$

The 12-15 steepest points of the K-M function were selected. Points that were far away from the others (i.e. local plunges) were removed and not considered, as a part of the manual quality control of the method. The remaining points from the selection were used as points in the MS Excel functions SLOPE and INTERCEPT, that corresponds to the a and b in the linear equation

$$y = ax + b,$$

respectively. Finally, to find the bandgap the equation was solved for x when $y = 0$. The bandgap value was then displayed in the chart title for each of the catalysts. A graphical example is shown in figure 14. All the operations mentioned above was scripted as MS Excel Macros in Visual Basic for Applications (VBA). This has been an attempt to automate the bandgap calculations described in section 3.9.

It has been difficult to obtain knowledge in the literature of how others have determined the equation for the linear part of the Kubelka-Munk curve, other than just making a

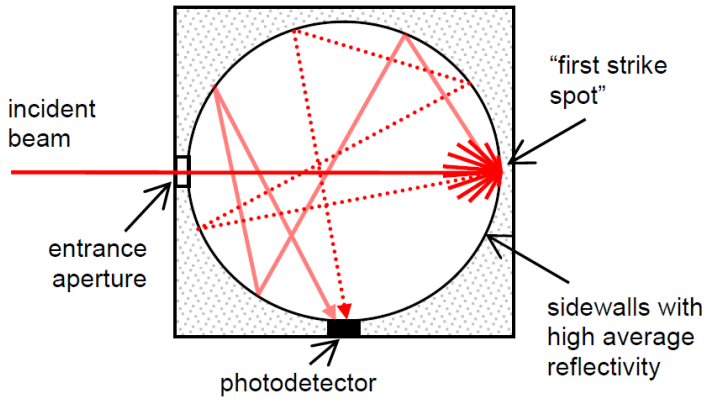

Figure 13 – *Principal illustration of the PerkinElmer 100 mm integrating sphere, as explained in figure 12.*

visual extrapolation to the x-axis. In agreement with the supervisors, the described method was applied for all bandgap estimations.

4.3 Photocatalytic reactor

A photocatalytic reactor was built specifically for the work in this project. The purpose of the reactor was to test the radical production for some of the most promising material samples provided by KeraNor.

The reactor basically consisted of a cylindrical water reservoir with a spinning disc connected to an electromotor through a vertical axle in the centre bottom of the reservoir. The circular material sample was centered and attached to the spinning disc. A bracket for the LED light was put on top of the reservoir, and a LED disc provided by PW Circuits LTD was placed in the bracket. A principal drawing and a photo of the reactor is shown in figure 15a and 15b.

Two LED discs were provided by PW Circuits LTD, one at 365 nm and the other at 375 nm. The latter was chosen for the experiments, as it had the highest intensity of the two, thus would yield the highest treatment efficiency. A control unit was also provided with the LED discs, and several combinations of settings were possible. The front panel of the control unit is shown on figure 16.

Next, the intensity of the UV LED lamps was measured at different distances. The intensity was measured with a RM-12 radiometer with a UVA+ sensor, with the detection range of 330-455 nm. From the response curve a ~90 % response for the 375 nm wavelength

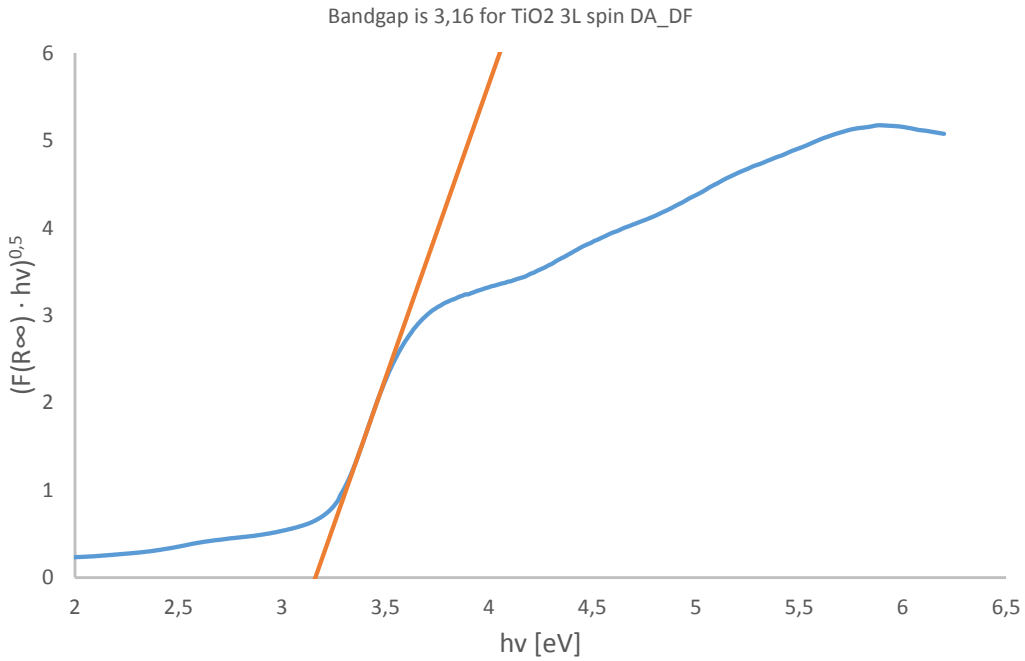

Figure 14 – *Example of a Kubelka-Munk plot for determination of the bandgap energy for the given photocatalyst. The intercept of the linear extrapolation with the x-axis represents the bandgap.*

light is obtained. The data sheet for the radiometer is shown in appendix C. The results from the intensity measurements are shown in the results section.

4.3.1 Experimental setup and procedure

The starting concentration C_0 was decided to be ~100 µg/L. However, C_0 was not identical for each run of the reactor, as there were some inaccuracies in the measuring. This was easily corrected by using the conversion $\tau = \frac{C_0 - C}{C_0}$ instead of the absolute removal retrieved from $-\frac{dC}{dt}$.

After some trial and error 100 mL was chosen as the water volume to be treated in the reactor. The spinning velocity was set to "4.8" on the display on the control unit; a value that has no physical meaning.

In order to get some momentum in the experiments, the highest intensity possible was chosen for the LEDs, together with a constant photon flux. This corresponds to the settings 5 and C for the intensity and irradiation mode, respectively.

(a) *Picture of the reactor setup.*

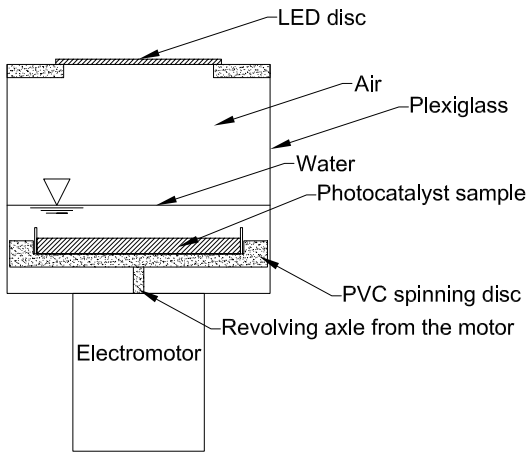

(b) *Principal drawing of the reactor*

Figure 15 – *Figure (a) shows a photo of the reactor setup with the reactor, electromotor and the control box as it is in the lab. The LED disc was not mounted when the image was shot. Figure (b) is a principal drawing of the reactor seen from the side.*

Procedure

The radical production procedure occurred in the following manner:

1. The reactor was rinsed with Milli-Q water, and gently wiped dry with paper.
2. The spinning disc was mounted to the vertical axle by a screw through the center.
3. 100 mL of a standard solution of ~100 µg/L pCBA was poured into the reactor.
4. The first of seven samples was drawn by a 100-1000 µL pipette from the water that was just poured into the reactor. The sample volume was 600 µL (as for the other samples), and was put into a vial of 1.5 mL.
5. The vial was then put into a dark cabinet.
6. The LED bracket was put onto the reactor, and the LED disc was put on top of it.
7. The control units for the electromotor and the LEDs were used to initiate the spinning and the irradiation. The entire procedure from point 3 to the initiation of the instruments took about 30 seconds.
8. After another 15, 30, 60, 120, 180 and 240 minutes water from the reactor was sampled. Before each sample the light and spinning were turned off, and the LED

Figure 16 – *Front panel of the LED control box.*

disc removed in order to get access to the reactor water. Immediately after each sampling the LED was mounted and the spinning and light turned on again.

9. The HPLC analysis of the samples was commenced after around 180 minutes of reactor time because it was rather time demanding (1-2 hours). The sample taken after 240 minutes was put into the HPLC immediately to be a part of the same testing sequence. Further, a Milli-Q sample was added to the end of the sequence to check for abnormalities with the analysis.

4.4 High-Performance Liquid Chromatography (HPLC)

High-performance liquid chromatography is an analytical method used to separate, identify and quantify substances in a liquid mixture. Therefore, it is both a quantitative and a qualitative method. In the current experiment it is used for establishing the concentration of p-chlorobenzoic acid (pCBA) in water samples ranging from 2 to 200 µg/L.

First, a calibration curve was made. One liter of Milli-Q was poured into a bottle. 2.00 µg of powdered pCBA was attempted measured, but due to practical limitations of the weighing the stock solution became 2.21 µg/L instead. This stock solution was used for all the experiments, not only the calibration curve.

From the stock solution, eight standard solutions of 0, 5, 10, 25, 50, 75, 100 and 200 µg/L were prepared. The exact concentrations of the standard solutions are displayed in appendix A. The corresponding output areas from the HPLC are also shown there.

The area was plotted against concentration in MS Excel, and a linear trendline was obtained with the built-in trendline function, as shown in figure 17.

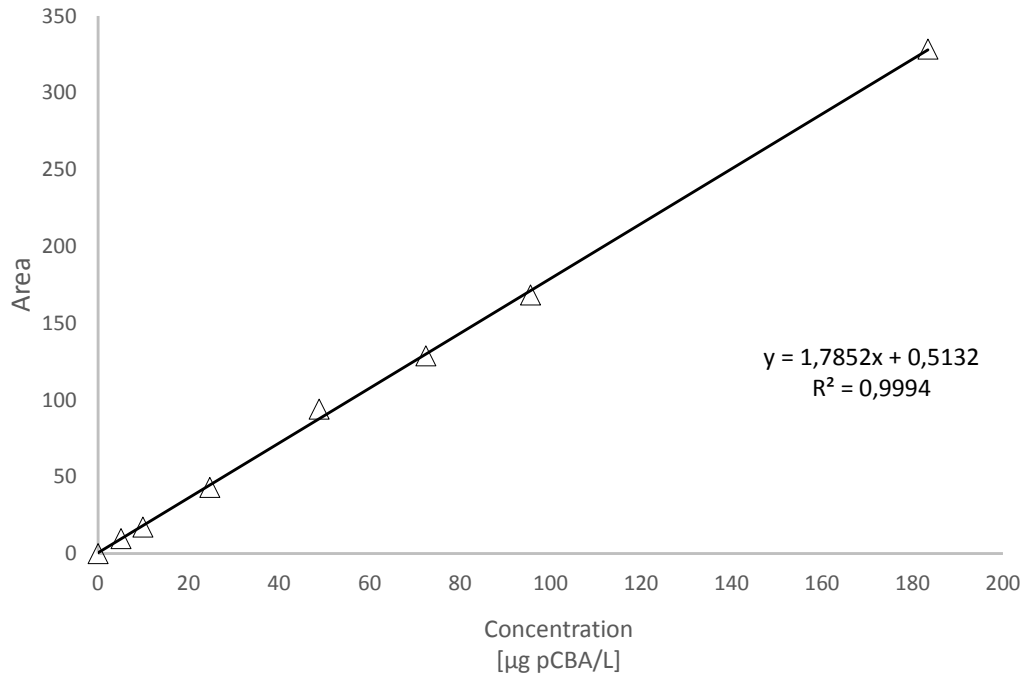

Figure 17 – *Calibration curve for pCBA measurements in the HPLC.*

The linear equation for the trendline was

$$y = 1.7852x + 0.5132 \tag{11}$$

With an R^2 value of 0.9994. This implies a very good and precise calibration curve. The water samples of 600 µL from the reactor could now be calculated.

From the 600 µL samples 300 µL was withdrawn in the HPLC and injected into the mobile phase. The mobile phase consisted of 42 % acetonitrile and 58 % phosphoric acid buffer solution at pH 2. Next, the mobile phase reached the stationary phase in the column. Inside the stationary phase the different compounds were separated before they exited the column and passed a sensor.

The output from an HPLC analysis is a curve with a peak corresponding to the time the pCBA uses to go through the column of the HPLC with the given settings, as shown in figure 18. The area under this ”peak part” of the graph is integrated. This area corresponds to the remaining concentration of pCBA, calculated from the calibration curve equation (eq. 11).

Contaminants injected into the mobile phase absorbs light at different wavelengths. pCBA absorbs light at approximately 239 nm; hence, if the area under the peak part of

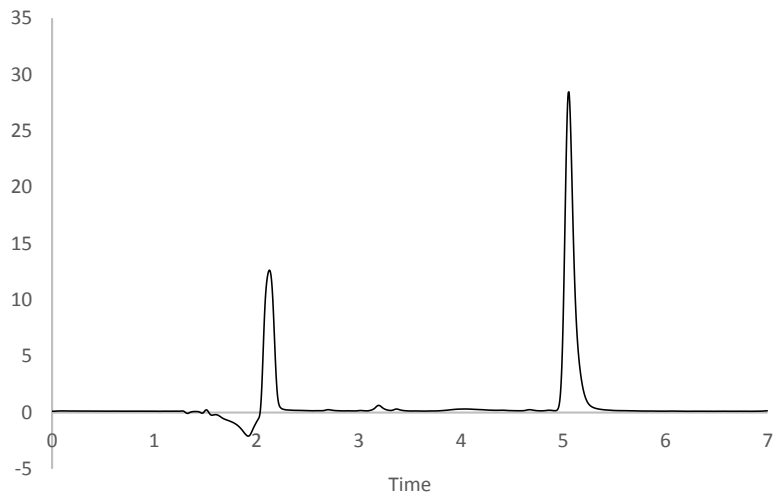

Figure 18 – *Example of an output curve from a HPLC analysis. The area under the second peak corresponds to the volume of pCBA passing by the column sensor. As more pCBA is removed from the water, the smaller this area becomes.*

Table 4 – *The HPLC output table corresponding to the output curve from fig. 18. The pCBA concentration is calculated from eq.* (11)*. It is the second peak that pCBA is accountable for.*

Peak number	Time of peak	Area	Height	Concentration
1	2.13	105.93	13.85	-
2	5.05	177.31	28.34	99.04

the curve consists of other wavelengths than from the 239 nm region, it is impossible to establish the correct area (and consequently the correct concentration). It is, in other words, possible to get an absorbance spectrum for each time step in the HPLC analysis, and this spectrum reveals information about the species that are present in the water.

Further, the ratio between the solvents (ACN and PO_4 buffer) has been chosen with great care, after extensive trial-and-error, in order to avoid peaks from other species in the water at the same time. The analyses showed stable results with little absorption at other wavelengths.

4.4.1 Determination of the detection and quantification limits

To ensure correct measurements it is important to determine the detection limit (DL) and quantification limit (QL) for the instruments used in analytical chemistry, especially when the concentrations of interest are close to the DL and QL. In this case the DL and

QL for the HPLC should be established, because the QL has been reported to lay between 10 and 40 µg/L for pCBA in other HPLC instruments (Huber et al. 2003).

The DL tells us the lowest concentration that is detectable by the HPLC, whereas the QL says something about the lowest concentration that can be quantified within a given variation criterion.

A method to perform such a determination was provided by one of the supervisors for this thesis. To find the detection limit the following work was executed:

1. Ten sample replicas of a known pCBA concentration were prepared and analyzed in the HPLC. All the samples had a volume of 600 µL and were taken from the same standard solution. This was done to avoid errors created by the slightly different dilution of the stock solution if several standard solutions had to be made.
2. The area of the pCBA in the HPLC analysis from each replicate was converted to concentration utilizing the calibration curve.
3. The average $\overline{x} = \frac{\sum_{i=1}^{n} x_i}{n}$ for all the concentrations x_i was calculated.
4. The standard deviation $S(n) = \sqrt{\frac{\sum_{i=1}^{n} (\overline{x} - x_i)^2}{n-1}}$ was calculated for the ten samples (n = 10).
5. The detection limit was estimated by calculating $DL = 3 \cdot S(n)$.
6. The quantification limit was estimated by calculating $QL = 10 \cdot S(n)$.
7. The conformity ratio (R) was calculated for the given concentration $R = \frac{\overline{x}}{3 \cdot S(n)}$.

The criterion for whether the estimated QL and DL values are valid or not, depends on the R value:
If $4 < R < 10$: the selected concentration is valid, and the QL and DL values are determined.
If $R < 4$: the QL and DL values are higher than the analyzed concentration, and a higher concentration must be checked.
If $R > 10$: the QL and DL values are lower than the analyzed concentration, and a lower concentration must be checked.

The results from those tests are shown in table 5. As clearly shown in the right column in table 5 all the concentrations were higher than the detection limit. Unfortunately, the software provided with the HPLC restricted integration of peaks with an area smaller than a given value. The software could be manipulated to integrate smaller peaks, but only with a great deal of trouble, even for the 2.00 µg/L standard solution. For lower concentrations it is very likely not possible to get the areas integrated; hence, the attempt to find the detection limit was brought to a halt.

Table 5 – *Detection and quantification limit test for the HPLC*

Concentration [µg/L]	$\overline{x}$	S(n)	QL	DL	R	Conclusion
5.01	4.9525	0.0132	0.132	0.040	125	Too high
3.50	3.4539	0.0335	0.335	0.101	34	Too high
2.00	1.8341	0.0137	0.137	0.041	45	Too high

Nevertheless, the detection limit could positively be concluded to be lower than 2.00 µg/L, and thus far below the concentration range for the experiments conducted in this thesis.

4.5 Production methods

KeraNor produced the materials that were analyzed and tested in this thesis. Due to the possibility of a patent application in connection with this project, a detailed description of the production method will not be presented here.

What could be said without disclosing any secrets is that a sol-gel method for the production of the photocatalysts was applied. This is a technique that offers low costs, simple processing, good compositional and stoichiometric control, as well as a large surface area of the end product (Deng et al. 2011). For the first photocatalysts received from KeraNor a dip coating technique was used. Later a spin coating technique was employed and preferred due to its superior properties regarding uniformity and reproducibility.

Both dense and porous alumina, as well as stainless steel were used as support materials. After some testing in KeraNor's own lab, dense alumina was selected as the most suitable support material for further testing. Stainless steel showed results that were somewhat promising, but due to issues with diffusion of steel molecules into the TiO_2 bulk, the material was conductive and unsuitable for photocatalysis. Until the diffusion issue is resolved, dense alumina will be the support material used further on in this project.

4.6 Analytical methods that should be applied

Desirably, additional analytical methods should have been applied for the characterization of the photocatalysts. This was not practically feasible in such a short timespan, and that made it difficult to discuss anything about the structure, thickness of coating layers, crystallinity, anatase/rutile ratio, distribution of dopant ions/atoms, uniformity, photoactivity in visible light and other important physicochemical properties of the catalyst.

To establish the impact different modifications of the photocatalyst have on the physicochemical properties of the catalyst, some of the highly advanced analytical methods such as the methods described in Dolat et al. (2015) should be applied:

- SEM with EDS (to perform elemental microanalysis)
- EPR-AFMR (to measure radical production)
- XRD (to characterize the crystalline structure)
- ICP-OES (to measure trace metal concentrations in the structure)
- UV-vis/DR (to characterize the light absorption ability)
- N_2 adsorption/desorption at 77 K (to determine the specific surface area)
- Elemental analysis

5 Results and discussion

The purpose of the experiments is to test whether addition of metal dopants to the photocatalytic semiconductor TiO_2 can reduce the bandgap energy, and at the same time enhance the radical production.

The result part of the thesis contains results from the spectrophotometric analyses of numerous TiO_2 materials with different doping and configurations. The metal dopants examined were mainly iron (Fe) and manganese (Mn) in different configurations.

Further, a comparison of the photocatalytic activity under UV irradiation (375 nm) for a selection of the materials follows. Optimally the catalysts should have been tested under visible light irradiation as well, but that was unrealistic in such a short time, and the LED lamps with 400 nm wavelength did not arrive in time from the manufacturer.

Next, the main part of the discussion was intended to be a thorough discussion of why the catalysts perform the way they do. Unfortunately, this part will be shortened due to difficulties reproducing the photocatalytic activity for the catalysts. The reference sample, for instance, varied from ~40% to ~60% removal of pCBA from one run to the other. Until the issue with fluctuating results is resolved by modifying the reactor design, the radical production results are too uncertain to discuss.

Some suggestions for the sources of error are discussed, and this will hopefully give some hints for further development of the method and reactor design used in this project.

Description of the different TiO_2 samples

TiO_2 samples with three different support materials were provided by KeraNor. The support materials were stainless steel (SS), purous alumina (PA) and dense alumina (DA). An overview of the bandgaps for all the tested samples are displayed in the tables 6, 7 and 8. The catalysts have unfortunately slightly confusing names in these tables. The main rule is that all layers on top of the support material consist of TiO_2 and often a dopant. The first layer (directly on the support material) is named first.

Take "TiO_2-TiO_2-Fe 0.5M spin" as an example. The two first layers of coating consist of pure TiO_2, and the third (and last) layer consists of TiO_2 doped with iron (Fe) at the concentration of 0.5M. This is illustrated on figure 19. "Spin" refers to the method used to apply the coating.

5.1 Bandgap results

Bandgap analyses were performed for numerous samples with the support materials stainless steel (SS), porous alumina (PA) and dense alumina (DA). The results are presented in table 6, 7 and 8.

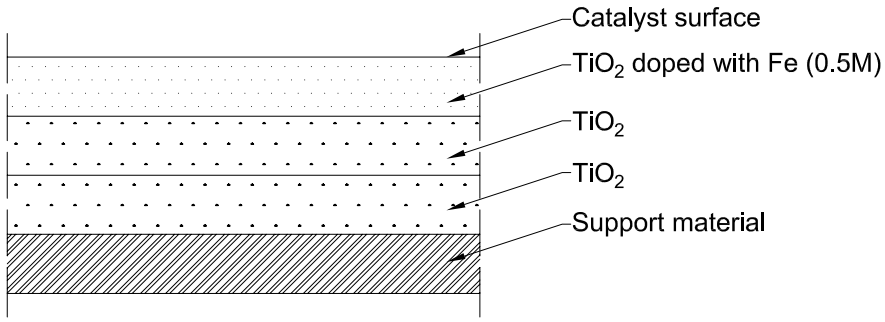

Figure 19 – *Sketch of the physical structure for the example photocatalyst TiO_2-TiO_2-Fe 0.5M spin.*

5.1.1 Analyses of stainless steel samples

Quite some effort was put into spectrophotometric analyses of the stainless steel samples. However, none of the samples had a promising shape in the Kubelka-Munk plot. It was suggested that extensive diffusion of steel molecules into the TiO_2 lattice and surface was occurring. Consequently, a diffusion barrier of silica SiO_2 was applied between the steel and the TiO_2 layers. Still, the Kubelka-Munk plots did not have a shape anywhere near a regular TiO_2 plot, as compared in figure 20.

The porous alumina sample used as an example has a shape that coincides with nearly any other of the TiO_2 catalysts analyzed for this thesis. As clearly shown, the curve drops down at around 3.5 eV, and the linear extrapolation ends up around 3.0 eV. On the contrary, the curve for the SS sample has no distinct drop, and it is concluded that it does not show a semiconductive behaviour, which is necessary for photocatalysis to work.

Furthermore, in the documentation of the spectrophotometer it is clearly stated that if a sample has a specular behaviour, and not diffuse, the results will be faulty. Visually the SS samples look rather specular. This problem may be solved by using a specular reference material instead of the diffuse Spectralon standard.

Later, a simple test to check whether the diffusion barrier worked or not was performed with a conductivity measurement over the catalyst surface, and then compared to the backside conduction where there was no coating of any kind. It turned out that the material was just as conductive on the barrier side as on the non-treated side. On this basis it was concluded that the production method was not yet good enough to proceed with

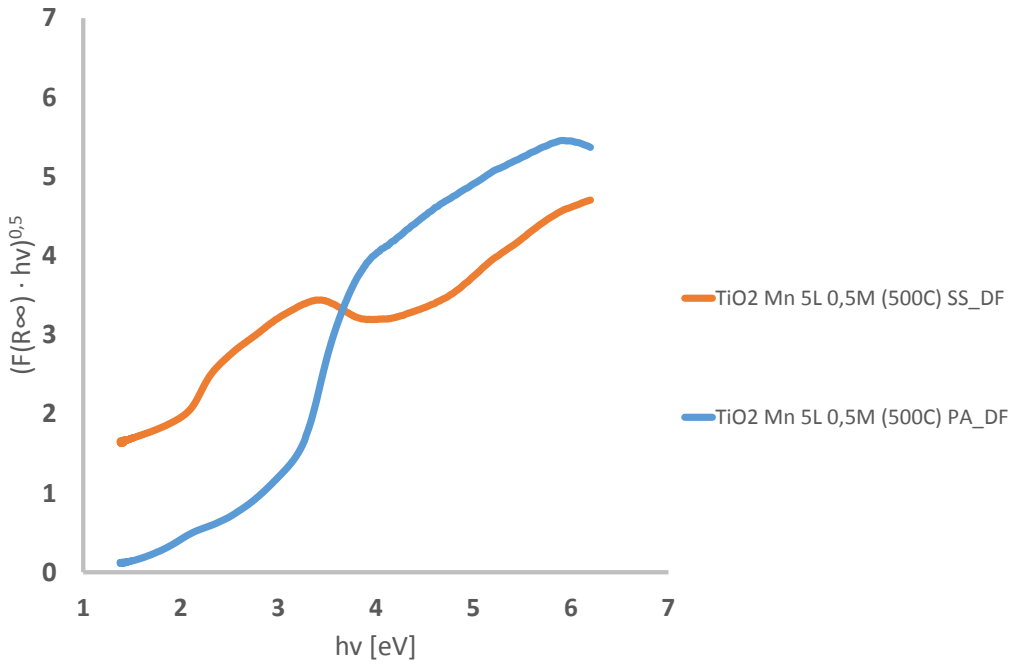

Figure 20 – *Comparison of a stainless sample and a porous alumina sample with the same doping applied. The blue curve represents the PA sample, and the red curve represents the SS sample. Large deviations from the SS to the PA sample is observed, making it probable that the SS sample is not acting as a photocatalyst.*

stainless steel as the support material, since a photocatalyst must be a semiconductor.

Table 6 – *Estimated bandgap energies for the stainless steel (SS) samples analyzed in the spectrophotometer. Most likely are all of the estimations incorrect, because the material is conductive.*

Entry	Photocatalyst	Bandgap [eV]	Coating method
1	SiO2-SiO2 (50-50 large-water)	-	Spin
2	SiO2-SiO2 (small)-TiO_2-TiO_2-TiO_2	2.63	Spin
3	SiO2 (large)-Mn-Mn-Mn 2M	2.52	Spin
4	SiO2-TiO_2-TiO_2-TiO_2	2.50	Spin
5	SiO2 (small)-TiO_2-TiO_2-TiO_2	2.48	Spin
6	ITO-TiO_2-TiO_2-TiO_2	2.28	Spin
7	SiO2-SiO2-TiO_2-TiO_2-TiO_2	2.21	Spin
8	Mn Mn (0.5M) TiO_2	2.02	?
9	SiO2-Mn-Mn-Mn 2M	1.76	?
10	Pure SS uncoated	1.70	-
11	ITO-ITO-TiO_2-TiO_2-TiO_2	1.49	Spin
12	TiO_2 Mn 5L 0.5M	1.00	?
13	TiO_2 Mn 3L 0.5M	0.54	?
14	TiO_2 TiO_2 Mn (0.5M)	0.32	?

5.1.2 Analyses of dense alumina samples

Results from the spectrophotometric analyses of the TiO_2 samples with dense alumina (DA) as support material is presented in table 7.

The dense alumina samples showed quite steady bandgap energies for all the spin coated samples, with a variation between 3.11 and 3.22 eV from entry 3-11. However, the two dip coated samples with three and five layers of Mn doped TiO_2 had a significantly decreased bandgap, with a bandgap energy of 2.89 and 2.96 eV, respectively. From the Tauc plot of TiO_2 Mn 3L 0.5M one can see that the curve apparently has two different bandgaps, as shown in figure 21.

However, good explanations in the literature was not found for such events, and lack of proper analytical experiments to study the catalyst structure and surface in this thesis leaves nothing but assumptions of the cause. As described in section 3.5, doping with metal ions will generally decrease the bandgap.

Anyway, a possibility is that the dip coating of the material has left the dopant less uniformly distributed than samples that are spin coated. Further, areas with clusters of

Table 7 – *Estimation of the bandgap for the dense alumina (DA) samples analyzed in the spectrophotometer.*

Entry	Photocatalyst	Bandgap [eV]	Coating
1	TiO_2 Mn 3L 0.5M	2.89	Dip
2	TiO_2 Mn 5L 0.5M	2.96	Dip
3	Mn-Mn-Mn 0.5M	3.11	Spin
4	Fe-Fe-Fe 0.5M	3.12	Spin
5	TiO_2-TiO_2-Mn 0.5M	3.14	Spin
6	**TiO_2 3L**	**3.16**	Spin
7	Fe (0.1M)-TiO_2-Sc 0.5M	3.16	Spin
8	Fe (0.1M 100%)-TiO_2-Sc 0.5M	3.17	Spin
9	Mn (0.5M)-TiO_2-Sc 0.5M	3.18	Spin
10	TiO_2-TiO_2-Fe 0.5M	3.19	Spin
11	Fe (0.1M 50%)-TiO_2-Sc 0.5M	3.22	Spin
12	Pure DA (no coating) 1	4.02	-
13	Pure DA (no coating) 2	4.02	-

dopant will narrow the bandgap for that specific part of the catalyst. Areas with lower concentrations will not experience the same narrowing, and will therefore have a higher bandgap, thus the second bandgap appears.

However, by having too high concentrations of a dopant, the recombination rate will increase dramatically, as discussed in section 3.5.3. Next, in the experiments conducted for this thesis, the radical production results for the highly Mn doped samples showed no photocatalytic activity at all. Certainly, too much weight should not be put on those results, as they were not reproducible. This issue will be addressed later.

Further, several samples with the combination Mn/Sc and Fe/Sc were tested for bandgap. Surprisingly, none of them yielded any narrowing of the bandgap. Considering the discussion in section 3.5.3 about scandium doping, the reason could be that the scandium concentration is in fact too low. Low concentration doping of scandium interrupts the crystallization of anatase cells, and creates a large number of defects working as recombination centres. However, an optimal doping concentration of scandium will again decrease the bandgap and enhance the photocatalytic activity. Hence, it would perhaps be worth trying to increase the scandium concentration.

However, no earlier attempts of co-doping of scandium with either manganese or iron were found in the literature, making it hard to conclude with how those ions have interacted and affected the bandgap.

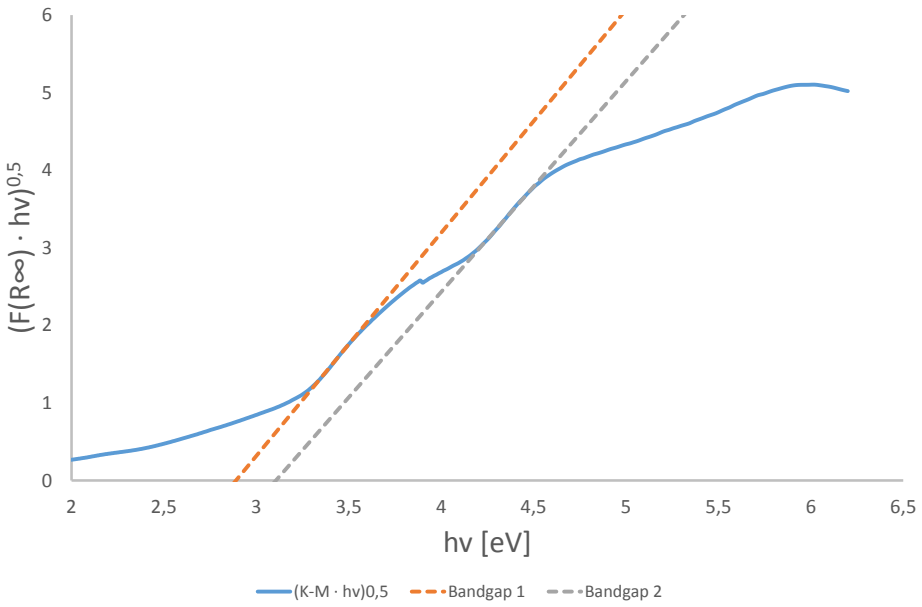

Figure 21 – *Tauc plot of a dip coated TiO2 Mn 3L 0.5M sample, with indications of two bandgaps.*

5.1.3 Analyses of porous alumina samples

The results from the spectrophotometric analyses of a selection of the the porous alumina samples are shown in table 8. The rest is shown in appendix B.

It is easy to see that doping with low concentrations of manganese (0.1M) in entry 6 gives only a small decrease in the bandgap compared to the reference in entry 9. There is, however, a clear tendency that when the concentration increases, the bandgap decreases correspondingly. This is consistent with the general observation in the literature, that any doping will narrow the bandgap, as discussed earlier in section 3.5.

Further, a discrepancy in the bandgap between entry 3 and 5, materials with the same doping applied, is observed. This could be caused by differences in the heating and calcination process, leading to deviations in the crystallinity or distribution of dopant in the lattice and surface of the catalyst. The material in entry 3 is square shaped, while entry 5 is circular. Incidentally, the circular sample is thicker than the square. It could be argued that this influences the stability of the anatase phase in the TiO_2 during the heating process, as anatase is known to have far less thermal stability than rutile. Further, rutile has a lower bandgap than anatase, meaning that entry 3 could have a higher rutile to anatase ratio than entry 5.

Needless to say, these statements are solely assumptions due to the lack of structural

Table 8 – *Bandgap results for the porous alumina (PA) samples analyzed in the spectrophotometer. The reference sample is shown in bold font in entry 9.*

Entry	Photocatalyst	Bandgap [eV]
1	Mn-Mn-0.5M-TiO_2	2.95
2	TiO_2-Mn-5L-0.5M	2.96
3	TiO_2-Mn 3L-0.5M	3.00
4	TiO_2-TiO_2-Mn-0.5M	3.01
5	TiO_2-Mn-3L-0.5M (circular)	3.09
6	TiO_2-Mn-3L-0.1M	3.13
7	TiO_2-5L	3.13
8	TiO_2-3L	3.14
9	**TiO_2-3L circular**	**3.15**
10	TiO_2-3L-(700C)	3.15
11	TiO_2-3L-(600C)	3.16

and surface analyses of the material samples.

5.1.4 Reproducibility

The results from the bandgap analyses were reproducible, and showed little variance when replicated. Due to the extensive selection of materials to test and analyze, time did not suffice to duplicate or triplicate all of them. In fact, only a small selection was duplicated or triplicated to check the reproducibility of results. The bandgaps for those tests are shown in table 9.

Table 9 – *Bandgap of selected dense alumina photocatalyst samples that was duplicated or triplicated. All the coated samples are spin coated.*

	Bandgap [eV]			
Photocatalyst	Run 1	Run 2	Run 3	Error [%]
Fe-Fe-Fe 0.5M	3.12	3.08	3.07	0.96
Mn-Mn-Mn 0.5M	3.11	3.08	3.08	0.64
TiO_2-TiO_2-Mn 0.5M	3.14	3.14	3.14	0.00
TiO_2-TiO_2-Fe 0.5M	3.19	3.12	3.12	1.46
Pure DA	4.02	4.03	4.03	0.17
Pure SS 1	1.70	1.66	1.74	2.41
Pure SS 2	1.62	1.61	1.67	2.20

An example is shown in a Tauc plot on figure 22 where three spectrophotometric analyses were run on the same sample (triplicate). Replicate 1 and 2 were analyzed at the very same spot on the sample, whilst replicate 3 was analyzed another day, and at a different spot. The shape of the curve was identical for replicate 1 and 2, whereas replicate 3 deviated marginally from the two former.

For this specific example the bandgap energy for all three analyses was 3.14 eV (395 nm). This shows that the spectrophotometer is fully able to reproduce results with a very good accuracy.

Further, the two bottom photocatalysts in table 9 were both pure SS samples. All the spectrophotometric analyses for these samples were taken on different spots. This was done mostly to check the uniformity of the samples. However, the bandgap for the SS samples are not genuine. Steel is a conductive material, and not semiconductive. This makes them unsuitable for photocatalysis when they are not properly coated.

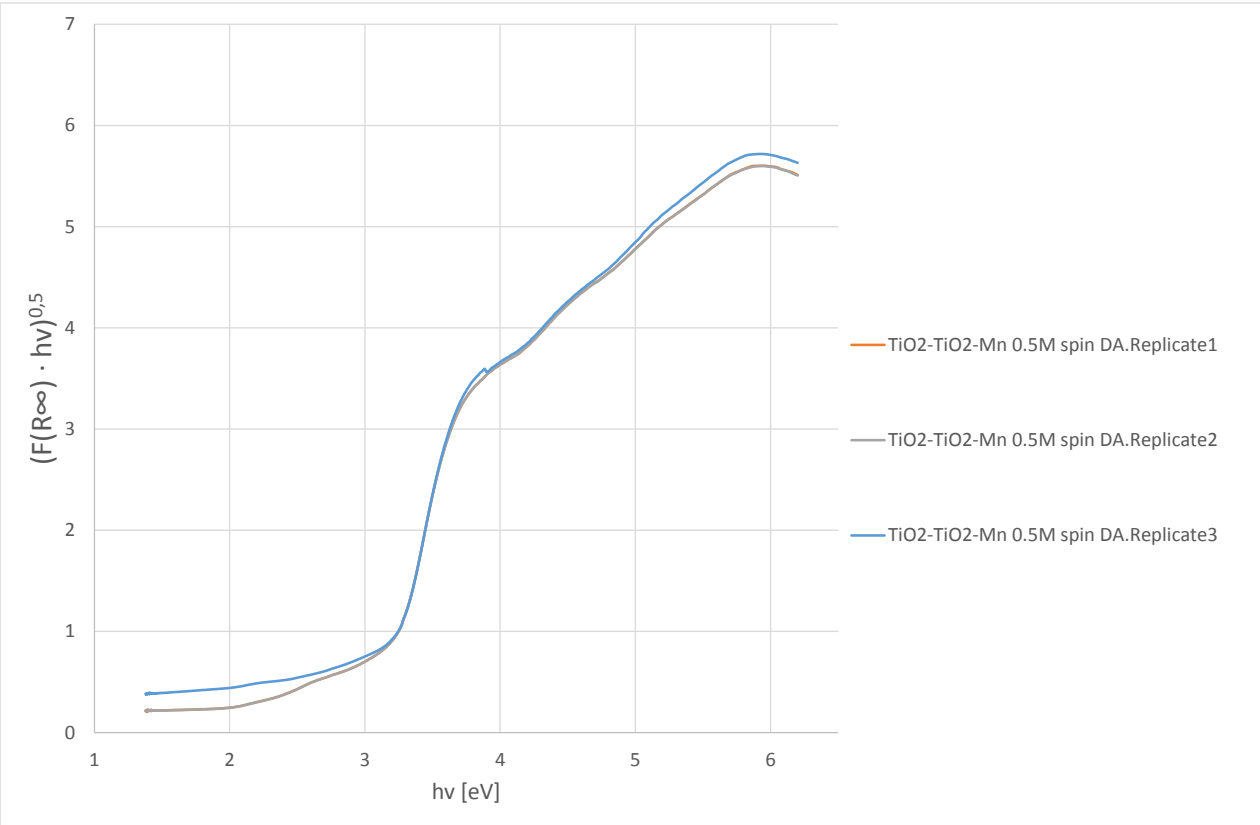

Figure 22 – *Reproducibility of the results from a spectrophotometric analysis of the sample TiO_2-TiO_2-Mn 0.5M spin coated dense alumina.*

5.1.5 Sources of error

Spectrophotometric analyses

Several sources of error could be conceivable for the spectrophotometric analyses. First, dust or dirt in the integrating sphere could affect the absorbance and give a distorted picture of the bandgap. Next, finger marks on the material samples could also change the absorbance and reflectivity properties.

Further, scratches on the Spectralon standard could possibly increase its absorbance slightly due to a larger surface area. Also dust and other contamination of the Spectralon could interfere with the reflectivity.

A small "bump" in the Tauc plot has been observed for some of the samples as well. This could not be explained by the author. However, it should not have any impact on the bandgap calculations anyway.

Otherwise, the results are very stable, and no obvious errors could be observed.

Reproducibility test

The small deviation for replicate 3 in figure 22 is most likely due to a slight non-uniform surface, and not inaccuracies in the spectrophotometric analysis itself. The curves for replicate 1 and 2, taken on the same spot, are identical (hence only one of the curves is visible on the figure). This proves that the instrument is very accurate.

However, the differences for the SS samples are a little bigger. Only two reasons comes in mind. First, it could be uneven distribution of metal alloying constituents that gives random light absorbance. Second, the method used for calculating the bandgap is quite sensitive to small changes in the steepness of the curve drop. If the curve does not have a sharp and distinct drop, it is probable that the material is not a photocatalyst, as the case is with pure stainless steel. Consequently, the linear part of the curve (if any) will have a very different gradient only with small changes in the curve appearance.

5.1.6 Statistical correlation between dopant properties and bandgap

A statistical model to express the correlation between the dopant properties and the bandgap should have been provided from the experimental work of this thesis. Dopant properties in question could have been concentration, distribution in different layers of coating, number of layers, support material, type of dopant (eg. Fe or Mn), etc. This would have been particularly useful to understand the influence of the different properties.

However, it is an absolute requirement that only one parameter change at a time. When two or more parameters change simultaneously it is impossible to tell which one has had (the largest) influence on the result. Regrettably, the samples provided for the testing did not fulfil this requirement, thence they were proclaimed inappropriate for such

a model.

Luckily, a similar analysis was performed by Prieto-Mahaney et al. (2009), as discussed in the literature review, section 3.4.1. They tested the six, according to them, most interesting properties of a TiO_2 photocatalyst regarding the photocatalytic activity: specific surface area, density of lattice defects, primary particle size, secondary particle size, anatase phase, and rutile phase.

They did, however, not conduct this analysis with doped TiO_2 samples. The only difference between the samples was the structures of the TiO_2. The most sensitive parameter for most of the photocatalytic reactions was the content of anatase.

5.2 Radical production results

The radical production did not give anything near the same result when experiments were replicated. Due to shortage of time, the radical production experiments were stopped when this was discovered as no obvious error could be identified. Consequently, the discussion part of this thesis will be dramatically shortened compared to what one could expect, and will mostly contain discussion about the possible sources of error.

5.2.1 Reproducibility

All the results from the radical production experiments are shown in table 10. Since one experiment took approximately five hours including preparations, there was not time to test all the samples. Many experiments were conducted before trying to reproduce any of the results. However, when the results from run 1 in entry 9 were ready, they showed a remarkable degradation of pCBA. Indeed, it was much better than the reference sample. According to most literature, that should not happen under UV irradiation.

On the basis of this single result, two reproduction runs were performed. From the results from run 1, 2 and 3 in entry 9 we observe that they do not coincide. Further, the reference sample experiment itself was duplicated, as seen in entry 2. Also this result deviated strongly from the first run. The results from the two runs from the reference sample in entry 2 are presented in figure 23.

As we see from the graph, both curves follow a first order reaction rate for the degradation of pCBA, with a very good fit. A first order reaction rate occurs when there is only the concentration of one species in the solution that influences the rate. In this case there are probably several species present, but the pCBA is by far the dominant one, at least in the beginning. Because the reaction in this experiment is not a true first order reaction, but behaves like one, it could be called a pseudo-first order reaction.

It is hard to explain how the two curves can have a nearly perfect fit, but still have so different reaction rates. Anyway, some of the possible error sources will be presented.

Table 10 – *Treatment efficiency for several doped TiO_2 photocatalysts with dense alumina as support material. All the samples are spin coated.*

		Treatment efficiency		
Entry	**Photocatalyst**	Run 1	Run 2	Run 3
1	TiO_2-3L (no light)	0.6 %	3.0 %	
2	**TiO_2-3L (reference sample)**	39.1 %	62.0 %	
3	TiO_2-TiO_2-Fe 0.5M spin	24.9 %		
4	TiO_2-TiO_2-Mn 0.5M spin	22.0 %		
5	Fe-Fe-Fe 0.5M spin	3.6 %		
6	Mn-Mn-Mn 0.5M spin	0.3 %		
7	Mn (0.5M)-TiO_2-Sc	32.9 %		
8	Fe (0.1M, 100%)-TiO_2-Sc	31.5 %		
9	Fe (0.1M)-TiO_2-Sc	58.6 %	27.4 %	33.6 %
10	Fe (0.1M, 50%)-TiO_2-Sc	34.1 %		

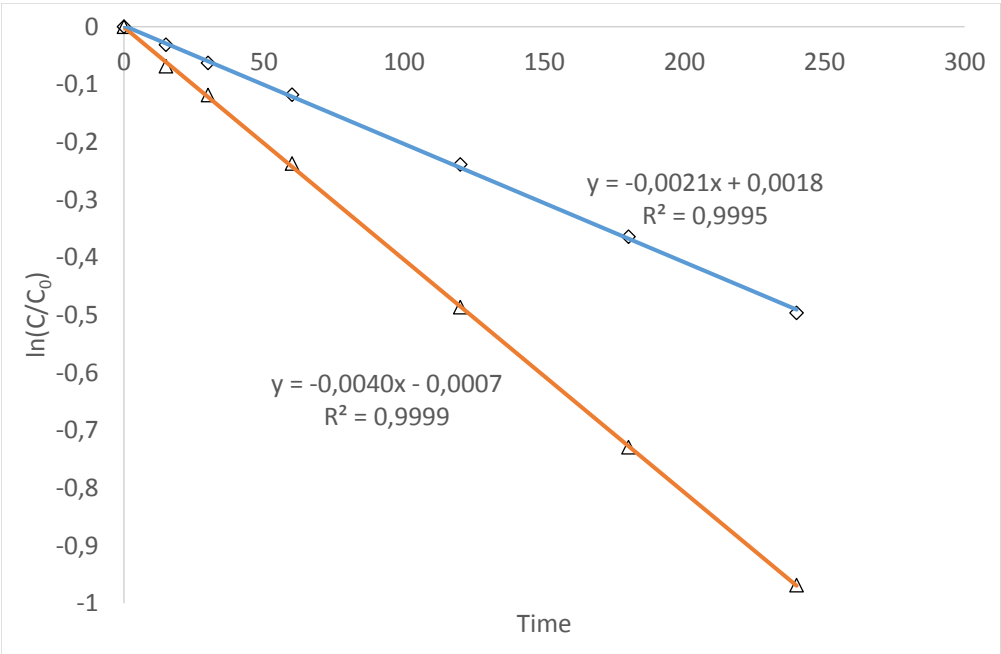

Figure 23 – *Pseudo-first order reaction rates were obtained for two identical experiments on TiO_2 3L on dense alumina support.*

5.2.2 Sources of error

After the reproducibility issue was discovered, very few ideas for the cause of the variations arose. In addition, there was too little time to explore those few ideas. Anyway, the main thoughts are:

- Oil or grease from the axle
- Glue dissolving in the reactor
- Inadequate mixing in the reactor
- Variations in the reaction pathway for the pCBA
- Influence of where in the reactor the sampling is done

Oil or other contaminants in the photoreactor

Small, black particles could be observed in the water volume during some of the photocatalytic experiments. This was at first not thought of as problematic since there was so little of it. The likely source of the black particles is the axle part of the reactor, as shown in figure 24. Since the pCBA concentration in the reactor was in the magnitude of µg/L, only a small amount of contamination would work as a scavenger, and "steal" the radicals from the pCBA. Consequently, the treatment efficiency could be dramatically affected. In addition, some glue used to attach some parts together could possibly dissolve slightly. The screws with the glue is also visible in figure 24.

Figure 24 – *Picture of the newly washed photoreactor. When it was flushed with ethanol and wiped with a white paper, the paper turned black, proving that this is likely to be a contamination source.*

Although the reactor wash flushed with ultrapure Milli-Q water twice between each experiment, it was probably not sufficient. Further, it must be said that no experiment has been conducted after the photoreactor was thoroughly rinsed with ethanol, due to the mentioned shortage of time; hence, other error sources could be responsible for the variations in the results.

Inadequate mixing

Again, shortage of time and eagerness to get the experiments going resulted in some flaws in the reactor design. First, the water surface was not horizontal during the photocatalytic experiments, as illustrated in figure 25. The reason for this is the revolving disc, dragging the water toward the walls. As a result, the light travelled through less water in the centre, probably making the treatment more effective here.

Additionally, water with an angle to the light will, according to Snell's law, refract the rays and further decrease the amount of photons reaching the catalyst surface, as shown in figure 26.

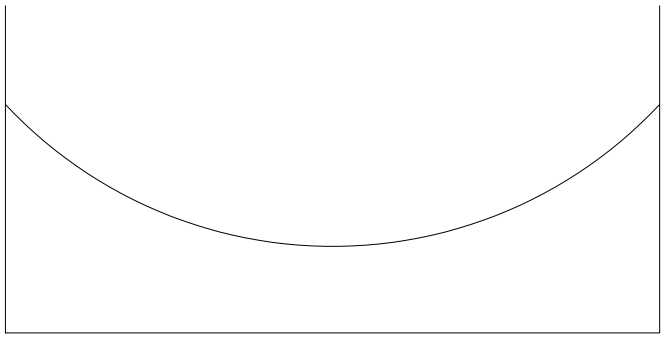

Figure 25 – *Principal sketch of the water surface in the photoreactor during a run, as seen from the side. Because of the spinning of the disc, water was dragged away from the centre of the material sample, making a meniscus in the water.*

Further, it was observed that the water in the centre was generally more stationary than the water near the walls. The black particles gathered mostly in the centre as well. If we assume that the photocatalytic activity is largest in the centre, as discussed above, then the scavenging effect is augmented by the oil particles (or other contaminants) gathering in the same area.

Varying reaction pathways for the pCBA

Since there is not one single product from the degradation of pCBA, but actually multiple possibilities, there are certainly many reaction pathways as well. Further, since radicals

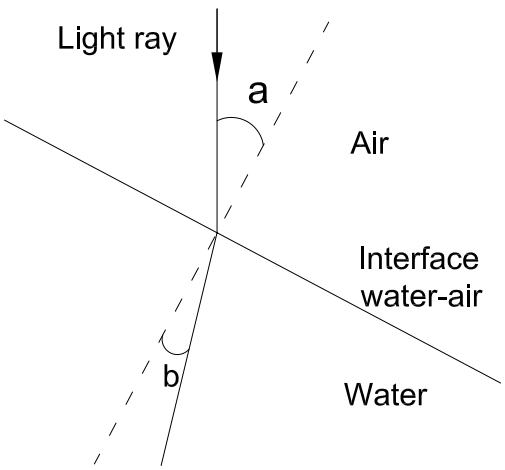

Figure 26 – *Refraction of light rays with an angle to the water surface, in accordance with Snell's law.*

from photocatalysis generally have no affinity with one species over another, the probability of one reaction to occur would be equal to another. Statistically speaking, the average reaction pathway should therefore even out in the long run. A reasonable assumption is that the varying reaction pathways for the pCBA would not yield such big differences in the degradation of pCBA observed from the experiments.

Location of sampling in the reactor

Based on the observation of the stationary water in the centre of the reactor during the experiments, it is suggested that the location of the sampling (i.e. where the pipette draws water in the reactor) could influence the results in the HPLC analysis. If the mixing is very inadequate, there should be a difference in the concentrations. This was in fact tested in a one-hour-run with sampling from the center and from the edge of the material sample. The results from this test are shown in table 11.

As the table shows, only very small variations were observed in this experiment. It is therefore concluded that the sampling location is of no significance for the results.

5.3 Correlation between bandgap energy and radical production

This section could have been the most important if the radical production showed valid results. However, as this is not the case a general discussion about correlations is presented instead.

First, a general impression after reviewing many papers and articles about doped TiO_2 is that the photocatalytic activity is decreased when the bandgap is narrowed. This means that, as an example, if the bandgap is altered from 385 nm to 420 nm from undoped to doped catalyst, the reaction rate could be reduced by for example 50 %. We also know

Table 11 – *Results from HPLC analysis of sampling at two different spots in the reactor, one in the center and one the edge of the material sample (i.e. close to the reactor wall). The material used for this experiment was the reference DA sample TiO_2 3L. The numbers in the table represents the measured pCBA concentrations.*

Minutes	**Edge**	**Center**	Error interval
0	104.24	104.13	104.18 ± 0.06 %
15	101.66	101.72	101.69 ± 0.03 %
30	101.05	101.27	101.16 ± 0.11 %
60	99.81	99.93	99.87 ± 0.06 %

that a photocatalytic reaction is strongly dependent on the light intensity, as explained in section 3.7 and from figure 9. Further, LED lamps have a significantly higher efficiency in the visible light spectrum than in the UV spectrum. If the extra light intensity for a 420 nm lamp can compensate for the loss of quantum yield (molecule converted per photon), this would be a better photocatalyst than the undoped TiO_2.

Without having any numbers for the increased efficiency for a LED from 375 to 420 nm, the photocatalytic activity is most likely decreased by 90 % for any photocatalyst. For instance, the example of an anion-doped TiO_2 presented in the literature review showed a 90 % reduction of activity already when the light exceeded 400 nm (Dolat et al. 2015).

In other words, it looks extremely difficult to develop a photocatalyst with anything near the same activity when visible light is used instead of UV light.

5.4 UV LED light intensity measurement

The distance from the UV light source to the material sample in the photoreactor was measured to be 7.5 cm. In order to check the intensity, light intensity for the UV LED with a wavelength of 375 nm was measured at different distances (including 7.5 cm), as shown in table 12.

It is obvious from the results that the distance from the light source to the material sample is crucial for the light intensity. When the first preliminary testing started, the distance was about 20 cm. At this distance very little degradation of pCBA took place. Later the distance was reduced to 7.5 cm simply by removing a part from the reactor. With this distance the results were acceptable.

5.5 Quantum yield calculation for reference sample

A quantum yield example for a reaction in this experiment could be estimated. In the beginning of the reactor time the dominant species is pCBA. After a few hours there

Table 12 – *Light intensity from the 375 nm LED disc as a function of the distance from the disc to the light sensor. The intensity was measured both in the centre and at the edge of the material sample.*

Distance [cm]	**Center [mW/cm²]**	**Edge [mW/cm²]**
3.0	3600	1710
5.0	1525	1008
7.5	927	713
12.0	375	324

should be several other species in the solution, and the calculations would be inaccurate. Thus, the removal of pCBA from 0 to 15 minutes will probably be the best measure to calculate the quantum yield.

Entry 2 run 2 (from table 10) on the pure TiO_2 sample is taken as an example. Firstly, the photonic flux φ is estimated. As recalled from section 3.2, this is calculated by

$$\varphi = \frac{I}{E} \cdot A_{surface}.$$

The pure TiO_2 3L DA sample has the surface area of $A_{surface} = \pi r^2 = \pi(\frac{7.6}{2})^2 \approx 45cm^2$. The average intensity is approximated to be the average of the edge and center intensity from table 12 (i.e. 820 mW/cm^2). All the light is assumed to be at 375 nm, hence the photon energy is

$$E \approx 1240/375 = 3.31\ eV \cdot 1.602 \cdot 10^{-19}\ J/eV = 5.30 \cdot 10^{-19}\ J.$$

The efficient photonic flux is then

$$\varphi = \frac{820 \cdot 10^{-3}\ J/s \cdot \mathrm{cm}^2}{5.30 \cdot 10^{-19}\ J} \cdot 45\ cm^2 = 6.96 \cdot 10^{19}\ s^{-1}$$

Next, the reaction rate denotes the conversion of molecules per second. This could be approximated the following way. First, the difference in mass of pCBA per second is found between 0 and 15 minutes from the experiments.

$$\frac{(104.29 - 97.40)\ \mu\mathrm{g/L}}{15\ min} \cdot 0.100\ L \cdot \frac{1}{60}\ min/s = 7.66 \cdot 10^{-4}\ \mu\mathrm{g/s}$$

Next, the expression is converted to mol/s:

$$n = \frac{m}{M} = \frac{7.66 \cdot 10^{-4} \text{ µg/s}}{156.57 \ g/mol} = 4.89 \cdot 10^{-6} \ mol/s$$

To find the number of molecules converted per second simply multiply with Avogadro's constant ($6.022 \cdot 10^{23} \ mol^{-1}$)

$$\text{\# of molecules converted per second} = 4.89 \cdot 10^{-6} \ mol/s \cdot 6.022 \cdot 10^{23} \ mol^{-1} = 2.94 \cdot 10^{18} \ s^{-1}$$

This number denotes the r in the quantum yield equation

$$QY = \frac{r}{\varphi} = \frac{2.94 \cdot 10^{18} \ s^{-1}}{6.96 \cdot 10^{19} \ s^{-1}} = 4.23 \cdot 10^{-2}$$

This calculation shows that the quantum yield for the pure TiO_2 in this experiment is consistent with (i.e. is in the same magnitude as) the literature, as discussed in e.g. section 3.2.2. Notably, no adsorption effect nor any influence of other contaminants in the water (e.g. oil or grease) is considered. However, the concentration numbers were retrieved from the experiment in entry 2 run 2 in table 10, with the highest pCBA degradation rate of all runs. This implies that the water was probably at its purest during this run (compared to the other runs), and that the influence of other contaminants was small.

6 Concluding remarks

6.1 Summary and conclusion

An attempt on establishing two main characteristics of doped titanium dioxide samples was conducted in this thesis. First, the bandgap was found with a spectrophotometer and some post-calculations, while the photocatalytic activity was measured with the help of a photoreactor and HPLC analysis of a radical-degradable contaminant. The spectrophotometric analyses conducted for this project could show that the bandgap of TiO_2 has in fact been narrowed after doping for nearly all samples. A few samples with manganese dopant have even reached 2.9 eV (425 nm). This is well inside the visible spectrum, and could utilize LED lamps with much higher efficiency than the 365 and 375 nm lamps provided for the testing in this thesis. However, great challenges with the reproducibility of radical production measurements has made it difficult to conclude about the photocatalytic activity. Still, there are indications that the most heavily doped samples do not show any photocatalytic activity. This could mean that the hole concept of doped TiO_2 is a trade-off between narrowing the bandgap and keeping the photocatalytic activity at a pleasant level.

6.2 Experimental setup

The spectrophotometric analyses showed very stable and reasonable results, and no modifications needed to be made for the work in this thesis.

Furthermore, the setup of the photoreactor was clearly not good enough. A combination of lack of experience in designing and delay in the delivery of parts for the reactor yielded very fluctuating results. Some possible sources of error were identified, and contamination by oil or grease from the axle in the reactor was concluded to be the most likely to distort the results.

6.3 Proposal for future work

A general impression from the literature and own experiments is that manganese, iron and other cationic dopants will decrease the photocatalytic activity so much that it is not feasible for application in water treatment. A shift toward non-metal doping, and possibly also co-doping with the combination of a non-metal and a metal, could lower the bandgap and increase the photocatalytic activity. This depends, obviously, on what the real goal for the project is.

If the main oxidative reaction is happening through the holes h^+ and not the hydroxyl radicals $OH^{\cdot}$, as suggested in the literature review, the adsorption of contaminants should

be considered as a vital property of the catalysts. Graphene is one of the additives that could enhance the adsorption and several other properties, but also activated carbon has been examined by some researchers, although this is not discussed in this thesis.

Regarding the photoreactor, several measures should be made. First, a thorough wash with alcohol should be performed regularly before starting experiments. Second, the glue mentioned in the bottom of the reactor should perhaps be reconsidered as the best for this purpose, as it dissolves slightly over time when submerged. Next, the LED disc could be placed lower in order to get a faster reaction rate, and consequently a more efficient procedure. This requires modifications on the reactor. Further, different intensities should be tested to see what impact this has on the reaction rate. Also LEDs with longer wavelengths should be interesting to test.

Finally, a good characterization of TiO_2 demands much more than spectrophotometric analyses and pCBA degradation analysis. In the literature most experiments are described with the use of several structural and elemental analyses (e.g. XPS) to make more qualified assumptions about the effect of dopants and the TiO_2 itself. To avoid pure guessing of why some things work and other don't, access to other analytical instruments should be a priority.

However, there is still a lot of vague formulations and qualified assumptions in the literature suggesting that this topic is still poorly understood even by the best experts who have been working with this for decades. On this basis the project team is wished the best of luck in finding a good configuration of photocatalyst, LED and reactor design for full-size applications.

References

Asahi, RYOJI et al. (2001). "Visible-light photocatalysis in nitrogen-doped titanium oxides". In: *science* 293.5528, pp. 269–271.

Asahi, Ryoji, Takeshi Morikawa, Hiroshi Irie, and Takeshi Ohwaki (2014). "Nitrogen-Doped Titanium Dioxide as Visible-Light-Sensitive Photocatalyst: Designs, Developments, and Prospects". In: *Chemical Reviews* 114.19, pp. 9824–9852.

Bignozzi, Carlo Alberto and Bruce D. Alexander (2011). *Photocatalysis*. Springer Berlin, Germany.

Bolong, N., A. F. Ismail, M. R. Salim, and T. Matsuura (2009). "A review of the effects of emerging contaminants in wastewater and options for their removal". In: *Desalination* 239.1–3, pp. 229–246.

Cavalheiro, AA et al. (2008). "Effect of scandium on the structural and photocatalytic properties of titanium dioxide thin films". In: *Journal of Materials Science* 43.2, pp. 602–608.

ChemSpider.com (2015). *4-Chlorobenzoic acid*. URL: `http://www.chemspider.com/Chemical-Structure.6079.html`.

Choi, Wonyong, Andreas Termin, and Michael R. Hoffmann (1994). "The Role of Metal Ion Dopants in Quantum-Sized TiO2: Correlation between Photoreactivity and Charge Carrier Recombination Dynamics". In: *The Journal of Physical Chemistry* 98.51, pp. 13669–13679.

Clément, Jean-Louis et al. (2005). "Assignment of the EPR spectrum of 5, 5-dimethyl-1-pyrroline N-oxide (DMPO) superoxide spin adduct". In: *The Journal of organic chemistry* 70.4, pp. 1198–1203.

Deng, Q. R. et al. (2011). "Mn-doped TiO2 nanopowders with remarkable visible light photocatalytic activity". In: *Materials Letters* 65.13, pp. 2051–2054.

Di Valentin, Cristiana and Annabella Selloni (2011). "Bulk and surface polarons in photoexcited anatase TiO2". In: *The Journal of Physical Chemistry Letters* 2.17, pp. 2223–2228.

Dolat, D et al. (2015). "Nitrogen-doped, metal-modified rutile titanium dioxide as photocatalysts for water remediation". In: *Applied Catalysis B: Environmental* 162, pp. 310–318.

Dong, Haoran et al. (2015). "An overview on limitations of TiO 2-based particles for photocatalytic degradation of organic pollutants and the corresponding countermeasures". In: *Water Research* 79, pp. 128–146.

Finkelstein, E, GERALD M Rosen, and ELMER J Rauckman (1982). "Production of hydroxyl radical by decomposition of superoxide spin-trapped adducts." In: *Molecular Pharmacology* 21.2, pp. 262–265.

Fox, Marye Anne and Maria T Dulay (1993). “Heterogeneous photocatalysis”. In: *Chemical reviews* 93.1, pp. 341–357.

Han, Wenya et al. (2004). “Photocatalysis of p-chlorobenzoic acid in aqueous solution under irradiation of 254nm and 185nm UV light”. In: *Water research* 38.19, pp. 4197–4203.

Henderson, Michael A (2011). “A surface science perspective on photocatalysis”. In: *Surface Science Reports* 66.6, pp. 185–297.

Herrmann, J.-M. (2005). “Heterogeneous photocatalysis: state of the art and present applications In honor of Pr. R.L. Burwell Jr. (1912–2003), Former Head of Ipatieff Laboratories, Northwestern University, Evanston (Ill).” In: *Topics in Catalysis* 34.1-4, pp. 49–65.

Herrmann, Jean-Marie (2010). “Photocatalysis fundamentals revisited to avoid several misconceptions”. In: *Applied Catalysis B: Environmental* 99.3, pp. 461–468.

Hirano, Masanori et al. (2005). “Scandium-Doped Anatase (TiO2) Nanoparticles Directly Formed by Hydrothermal Crystallization”. In: *Journal of the American Ceramic Society* 88.9, pp. 2604–2607.

Huang, Weiping et al. (2000). “Selective synthesis of anatase and rutile via ultrasound irradiation”. In: *Chem. Commun.* 15, pp. 1415–1416.

Huber, Marc M, Silvio Canonica, Gun-Young Park, and Urs Von Gunten (2003). “Oxidation of pharmaceuticals during ozonation and advanced oxidation processes”. In: *Environmental Science & Technology* 37.5, pp. 1016–1024.

Ibusuki, Takashi and Koji Takeuchi (1986). “Toluene oxidation on UV-irradiated titanium dioxide with and without O 2, NO 2 or H 2 O at ambient temperature”. In: *Atmospheric Environment (1967)* 20.9, pp. 1711–1715.

Ishibashi, Ken-ichi, Akira Fujishima, Toshiya Watanabe, and Kazuhito Hashimoto (2000). “Quantum yields of active oxidative species formed on TiO 2 photocatalyst”. In: *Journal of Photochemistry and Photobiology A: Chemistry* 134.1, pp. 139–142.

Izadifard, Maryam, Gopal Achari, and Cooper H Langford (2013). “Application of photocatalysts and LED light sources in drinking water treatment”. In: *Catalysts* 3.3, pp. 726–743.

Jenks, William S (2013). “Photocatalytic Reaction Pathways–Effects of Molecular Structure, Catalyst, and Wavelength”. In: *Photocatalysis and Water Purification: From Fundamentals to Recent Applications*, pp. 25–51.

Kawahara, Tetsuro et al. (2002). “A Patterned TiO2 (Anatase)/TiO2 (Rutile) Bilayer-Type Photocatalyst: Effect of the Anatase/Rutile Junction on the Photocatalytic Activity”. In: *Angewandte Chemie* 114.15, pp. 2935–2937.

Kumar, K Vasanth, K Porkodi, and F Rocha (2008). “Langmuir–Hinshelwood kinetics–a theoretical study”. In: *Catalysis Communications* 9.1, pp. 82–84.

Kumar, S Girish and L Gomathi Devi (2011). “Review on modified TiO2 photocatalysis under UV/visible light: selected results and related mechanisms on interfacial charge carrier transfer dynamics”. In: *The Journal of Physical Chemistry A* 115.46, pp. 13211–13241.

Kümmerer, Klaus (2011). “Emerging Contaminants versus Micro-pollutants”. In: *Clean–Soil, Air, Water* 39.10, pp. 889–890.

Lasa, Hugo de, Benito Serrano, and Miguel Salaices (2005a). “Establishing Photocatalytic Kinetic Rate Equations: Basic Principles and Parameters”. In: *Photocatalytic Reaction Engineering*. Springer, pp. 1–15.

— (2005b). “Novel photocatalytic reactors for water and air treatment”. In: *Photocatalytic Reaction Engineering*. Springer, pp. 17–47.

— (2005c). “Photocatalysts, Radiation Sources and Auxiliary Equipment for Photocatalysis”. In: *Photocatalytic Reaction Engineering*. Springer, pp. 49–62.

Li, Gonghu and Kimberly A Gray (2007). “The solid–solid interface: explaining the high and unique photocatalytic reactivity of TiO 2-based nanocomposite materials”. In: *Chemical physics* 339.1, pp. 173–187.

Linsebigler, Amy L, Guangquan Lu, and John T Yates Jr (1995). “Photocatalysis on TiO2 surfaces: principles, mechanisms, and selected results”. In: *Chemical reviews* 95.3, pp. 735–758.

López, Rosendo and Ricardo Gómez (2012). “Band-gap energy estimation from diffuse reflectance measurements on sol–gel and commercial TiO2: a comparative study”. In: *Journal of sol-gel science and technology* 61.1, pp. 1–7.

Lu, Max and Pierre Pichat (2013). *Photocatalysis and water purification: from fundamentals to recent applications*. John Wiley & Sons.

Mandelbaum, Pablo A, Alberto E Regazzoni, Miguel A Blesa, and Sara A Bilmes (1999). “Photo-electro-oxidation of alcohols on titanium dioxide thin film electrodes”. In: *The Journal of Physical Chemistry B* 103.26, pp. 5505–5511.

Molinari, Alessandra, Luca Samiolo, and Rossano Amadelli (2015). “EPR spin trapping evidence of radical intermediates in the photo-reduction of bicarbonate/CO 2 in TiO 2 aqueous suspensions”. In: *Photochemical & Photobiological Sciences* 14.5, pp. 1039–1046.

Mottley, Carolyn, Henry D Connor, and Ronald P Mason (1986). “[17 O] oxygen hyperfine structure for the hydroxyl and superoxide radical adducts of the spin traps DMPO, PBN and 4-POBN”. In: *Biochemical and biophysical research communications* 141.2, pp. 622–628.

Murakami, Yoshinori et al. (2007). “Can OH radicals diffuse from the UV-irradiated photocatalytic TiO2 surfaces? Laser-induced-fluorescence study”. In: *The Journal of Physical Chemistry C* 111.30, pp. 11339–11346.

Muryn, CA et al. (1991). “Step and point defect effects on TiO 2 (100) reactivity”. In: *Surface Science* 251, pp. 747–752.

Naito, Kazuya, Takashi Tachikawa, Mamoru Fujitsuka, and Tetsuro Majima (2008). “Real-time single-molecule imaging of the spatial and temporal distribution of reactive oxygen species with fluorescent probes: Applications to TiO2 photocatalysts”. In: *The Journal of Physical Chemistry C* 112.4, pp. 1048–1059.

Nakaruk, A et al. (2012). “Fe-doped and Mn-doped titanium dioxide thin films”. In: *Journal of sol-gel science and technology* 61.1, pp. 175–178.

Ni, Meng, Michael KH Leung, Dennis YC Leung, and K Sumathy (2007). “A review and recent developments in photocatalytic water-splitting using TiO2 for hydrogen production”. In: *Renewable and Sustainable Energy Reviews* 11.3, pp. 401–425.

Nosaka, Yoshio and Atsuko Y Nosaka (2013). “Identification and roles of the active species generated on various photocatalysts”. In: *Photocatalysis and Water Purification: From Fundamentals to Recent Applications*, pp. 1–24.

Nosaka, Yoshio et al. (2003). “Photocatalytic OH radical formation in TiO 2 aqueous suspension studied by several detection methods”. In: *Physical Chemistry Chemical Physics* 5.20, pp. 4731–4735.

Ohtani, Bunsho (2013). “Design and Development of Active Titania and Related Photocatalysts”. In: *Photocatalysis and Water Purification: From Fundamentals to Recent Applications*, pp. 73–102.

Oller, I, S Malato, and JA Sánchez-Pérez (2011). “Combination of advanced oxidation processes and biological treatments for wastewater decontamination—a review”. In: *Science of the total environment* 409.20, pp. 4141–4166.

Pichat, Pierre (2015). “A short overview of the state of the art and perspectives on the main basic factors hindering the development of photocatalytic treatment of water”. In: *Water Science & Technology: Water Supply* 15.1, p. 1.

Prieto-Mahaney, Orlando-Omar, Naoya Murakami, Ryu Abe, and Bunsho Ohtani (2009). “Correlation between photocatalytic activities and structural and physical properties of titanium (IV) oxide powders”. In: *Chemistry Letters* 38.3, pp. 238–239.

Rajeshwar, Krishnan and Jorge G Ibanez (1997). *Environmental electrochemistry: Fundamentals and applications in pollution sensors and abatement*. Academic Press.

Richardson, Susan D. and Thomas A. Ternes (2014). “Water analysis: emerging contaminants and current issues”. In: *Analytical chemistry* 86.6, 2813–2848.

Salvador, P (2007). “On the nature of photogenerated radical species active in the oxidative degradation of dissolved pollutants with TiO2 aqueous suspensions: a revision in the light of the electronic structure of adsorbed water”. In: *The Journal of Physical Chemistry C* 111.45, pp. 17038–17043.

Scanlon, David O et al. (2013). “Band alignment of rutile and anatase TiO2”. In: *Nature materials* 12.9, pp. 798–801.

Scopus.com (2015). *Publications on photocatalysis used for water treatment*. URL: `http://scopus.com`.

Serpone, Nick (2006). “Is the Band Gap of Pristine TiO2 Narrowed by Anion- and Cation-Doping of Titanium Dioxide in Second-Generation Photocatalysts?” In: *The Journal of Physical Chemistry B* 110.48, pp. 24287–24293.

Shaham-Waldmann, Nurit and Yaron Paz (2013). “Modified Photocatalysts”. In: *Photocatalysis and Water Purification: From Fundamentals to Recent Applications*, pp. 103–143.

Taborda, AV, MA Brusa, and MA Grela (2001). “Photocatalytic degradation of phthalic acid on TiO 2 nanoparticles”. In: *Applied Catalysis A: General* 208.1, pp. 419–426.

Tanaka, Keiichi, Mario FV Capule, and Teruaki Hisanaga (1991). “Effect of crystallinity of TiO 2 on its photocatalytic action”. In: *Chemical Physics Letters* 187.1, pp. 73–76.

Tauc, J, R Grigorovici, and A Vancu (1966). “Optical properties and electronic structure of amorphous germanium”. In: *physica status solidi (b)* 15.2, pp. 627–637.

Teh, Chao Min and Abdul Rahman Mohamed (2011). “Roles of titanium dioxide and ion-doped titanium dioxide on photocatalytic degradation of organic pollutants (phenolic compounds and dyes) in aqueous solutions: A review”. In: *Journal of Alloys and Compounds* 509.5, pp. 1648–1660.

The Gallup Organisation (2009). *Flash Eurobarometer on water*. Tech. rep. URL: `http://ec.europa.eu/public_opinion/flash/fl_261_en.pdf`.

Upadhyay, Ravi Kant, Navneet Soin, and Susanta Sinha Roy (2014). “Role of graphene/metal oxide composites as photocatalysts, adsorbents and disinfectants in water treatment: a review”. In: *RSC Advances* 4.8, pp. 3823–3851.

Veselinovic, M. (2015). “Ethiopia’s $5 bn project that could turn it into Africa’s water powerhouse”. In: *CNN.com*.

Wilke, K and HD Breuer (1999). “The influence of transition metal doping on the physical and photocatalytic properties of titania”. In: *Journal of Photochemistry and Photobiology A: Chemistry* 121.1, pp. 49–53.

Wols, BA and CHM Hofman-Caris (2012). “Review of photochemical reaction constants of organic micropollutants required for UV advanced oxidation processes in water”. In: *Water research* 46.9, pp. 2815–2827.

Yu, Jiaguo, Quanjun Xiang, and Minghua Zhou (2009). “Preparation, characterization and visible-light-driven photocatalytic activity of Fe-doped titania nanorods and first-principles study for electronic structures”. In: *Applied Catalysis B: Environmental* 90.3, pp. 595–602.

Zhiyong, Yu et al. (2007). “ZnSO 4–TiO 2 doped catalyst with higher activity in photocatalytic processes”. In: *Applied Catalysis B: Environmental* 76.1, pp. 185–195.

Zou, Zhigang, Jinhua Ye, Kazuhiro Sayama, and Hironori Arakawa (2001). “Direct splitting of water under visible light irradiation with an oxide semiconductor photocatalyst”. In: *Nature* 414.6864, pp. 625–627.

Appendix A Calibration curve for HPLC analyses

Table A1 – *Data for the calibration curve for HPLC measurements.*

Concentration [µg/L]	Area [-]
0	0
5.07	9.7
9.90	17.2
24.69	43.1
48.84	94.0
72.46	128.7
95.57	168.4
183.41	328.4

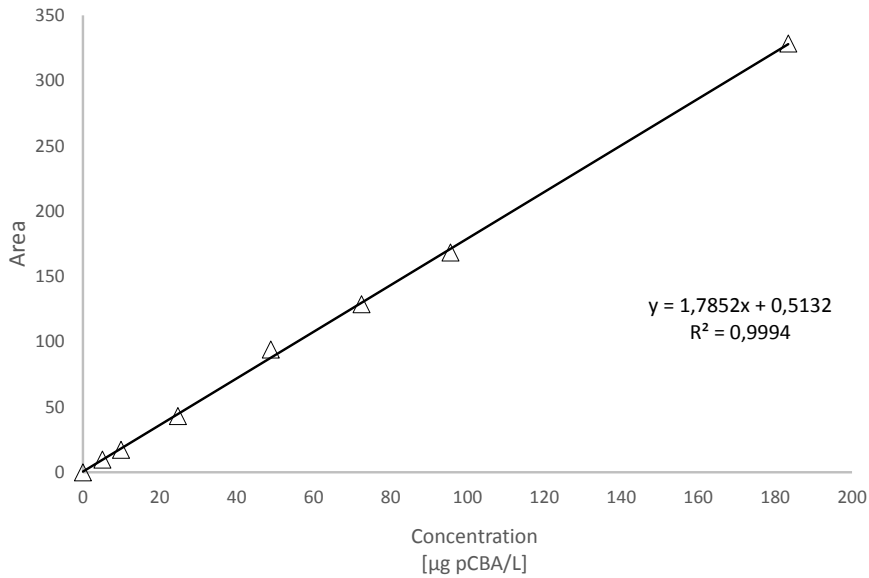

Figure A1 – *Calibration curve for the HPLC analyses.*

Appendix B Bandgap results for all samples

Table B1 – *Bandgap results for the porous alumina (PA) samples analyzed tested in the spectrophotometer.*

Photocatalyst	Bandgap [eV]	Photocatalyst	Bandgap [eV]
TiO_2-Mn	1.77	TiO_2-5L	3.13
TiO_2-Ag-low-5L	2.93	TiO_2-Mn-3L-0.1M	3.14
Mn-Mn-0.5M-TiO_2	2.95	TiO_2-Mn-3L-0.1M	3.14
TiO_2-Mn-5L-0.5M	2.96	TiO_2-Fe-2L-0.1M	3.14
TiO_2-Mn 3L-0.5M	3.00	TiO_2-Al-2L-0.2M	3.14
TiO_2-Pt-low-5L	3.00	TiO_2-Ag-3L-0.1M	3.14
TiO_2-TiO_2-Mn-0.5M	3.01	TiO_2-3L	3.14
TiO_2-Mn-3L-0.5M	3.07	TiO_2-Ag-low-1L	3.14
TiO_2-Mn-3L-0.5M	3.09	**TiO_2-3L circular**	**3.15**
TiO_2-Pt-low-1L	3.12	TiO_2-Al-2L-0.2M	3.15
TiO_2-Zr	3.13	TiO_2 3L (700C)	3.15
TiO_2-Mn-3L-0.1M	3.13	TiO_2 3L (600C)	3.16
TiO_2-Al	3.13	TiO_2-Fe-2L-0.1M	3.16
TiO_2-Ag-3L-0.1M	3.13	TiO_2-Ag	-

Table B2 – *Estimated bandgap energies for the stainless steel (SS) samples analyzed in the spectrophotometer. Most likely are all of the estimations incorrect, because the material is conductive.*

Entry	Photocatalyst	Bandgap [eV]	Coating method
1	SiO2-SiO2 (50-50 large-water)	-	Spin
2	SiO2-SiO2 (small)-TiO_2-TiO_2-TiO_2	2.63	Spin
3	SiO2 (large)-Mn-Mn-Mn 2M	2.52	Spin
4	SiO2-TiO_2-TiO_2-TiO_2	2.50	Spin
5	SiO2 (small)-TiO_2-TiO_2-TiO_2	2.48	Spin
6	ITO-TiO_2-TiO_2-TiO_2	2.28	Spin
7	SiO2-SiO2-TiO_2-TiO_2-TiO_2	2.21	Spin
8	Mn Mn (0.5M) TiO_2	2.02	?
9	SiO2-Mn-Mn-Mn 2M	1.76	?
10	Pure SS uncoated	1.70	-
11	ITO-ITO-TiO_2-TiO_2-TiO_2	1.49	Spin
12	TiO_2 Mn 5L 0.5M	1.00	?
13	TiO_2 Mn 3L 0.5M	0.54	?
14	TiO_2 TiO_2 Mn (0.5M)	0.32	?

Table B3 – *Estimation of the bandgap for the dense alumina (DA) samples analyzed in the spectrophotometer.*

Entry	Photocatalyst	Bandgap [eV]	Coating
1	TiO_2 Mn 3L 0.5M	2.89	Dip
2	TiO_2 Mn 5L 0.5M	2.96	Dip
3	Mn-Mn-Mn 0.5M	3.11	Spin
4	Fe-Fe-Fe 0.5M	3.12	Spin
5	TiO_2-TiO_2-Mn 0.5M	3.14	Spin
6	**TiO_2 3L**	**3.16**	Spin
7	Fe (0.1M)-TiO_2-Sc 0.5M	3.16	Spin
8	Fe (0.1M 100%)-TiO_2-Sc 0.5M	3.17	Spin
9	Mn (0.5M)-TiO_2-Sc 0.5M	3.18	Spin
10	TiO_2-TiO_2-Fe 0.5M	3.19	Spin
11	Fe (0.1M 50%)-TiO_2-Sc 0.5M	3.22	Spin
12	Pure DA (no coating) 1	4.02	-
13	Pure DA (no coating) 2	4.02	-

Appendix C Data sheets for lab instruments

PRODUCT NOTE

UV/Vis/NIR Spectroscopy

Key Features:

- Fully baffled detectors to prevent first strike light from reaching the detectors
- New design sample holder for improved sampling positioning
- Port fraction ratio of less than 3% meeting the requirements of many application needs
- Compatible with all high LAMBDA units 650, 750, 850, 950 and 1050 providing enhanced capability and performance to the line of LAMBDA units

100 mm Diffuse Reflectance and Transmission Integrating Sphere Accessory for All High-End LAMBDA Systems

Introduction

The 100 mm integrating sphere is a new design capable of being used with all high end LAMBDA systems. The module is available in two configurations which include PMT/Pbs detector and PMT/InGaAs detector providing the highest level of performance in a cost effective package for current LAMBDA users as well as new customers.

The new sphere design utilizes two measurement ports, (Transmission and Reflectance) with a dedicated reference beam only entrance only port thereby minimizing errors caused by port fraction ratios over 3% and increasing the dynamic range of the sphere over that of the 60 mm or 150 mm spheres. Detectors have been placed as to not interfere with either the transmission or reflectance port allowing clear access to position larger samples in the accessory. A convenient top access port allows easy access to view the beam position during alignment. This is essential when taking advantage of the transmission or reflectance only small spot kits or power sample holder. These kits are a cost effective solution allowing easy measurement of small samples as well as power type samples.

PerkinElmer®
For the Better

Figure C1 – *Data sheet for spectrophotometer with integrating sphere*

OPSYTEC PRODUCT INFORMATION

Opsytec Dr. Gröbel

Radiometric sensors

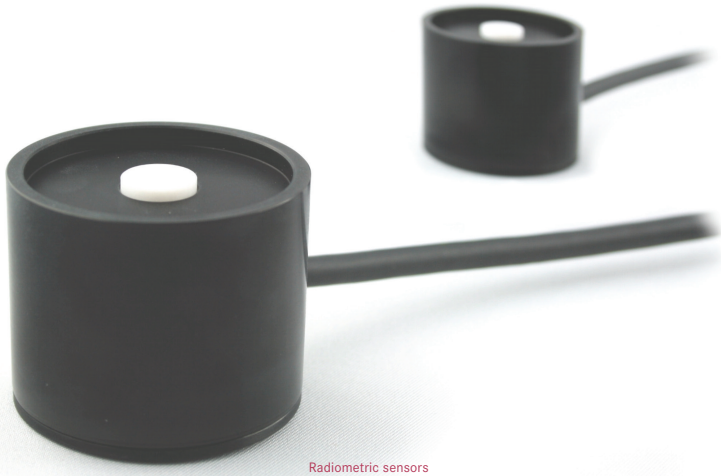

Radiometric sensors

Our radiometric sensors accurately measure the UV irradiance or illuminance with the RM-12 or RM-22 radiometer and the UV-MAT dose control. The built-in diffusers ensure the cosine correction that is required for non-vertical irradiation.

The sensors are calibrated with traceability to PTB (Physikalisch Technische Bundesanstalt, the German national test authority); after being calibrated, they are supplied with a factory calibration certificate. Excellent long-term stability is achieved through the use of appropriate materials. Of course, a repair and spare parts service is available for many years.

The integrated electronics produce a signal voltage that is transmitted to the radiometer. Various sensors can be used with a radiometer by means of internal electronics.

The sensor on the RM-22 is identified by additional memory, which also contains the calibration and the date of manufacture. Our range includes eight spectral ranges and four measuring ranges for the sensors.

This allows the radiometric sensors to be optimally adapted for the application.

Sensors to evaluate the biological effects of irradiation are also available. Going further if necessary, in special cases, the sensors are splash-proof in accordance with IP65 and available with advanced measuring and spectral ranges.

HIGHLIGHTS

- High-precision radiometric sensors
- Eight available spectral ranges
- Proven long-term stability
- Recalibrateable sensors
- Integrated electronics
- Different measuring ranges can be selected during order
- Customized adaption for special applications
- IP65 splashproof (optional)

Since 1981, Opsytec Dr. Gröbel GmbH manufactures UV sensors. All sensors are calibrated in our own laboratory.

Opsytec Dr. Gröbel GmbH
Goethestr. 17, 76275 Ettlingen, Germany

Phone +49 - 7243 - 94 783 - 50
Fax +49 - 7243 - 94 783 - 65

www.uv-groebel.com
info@uv-groebel.com

certified according DIN EN ISO 9001:2008

Figure C2 – *Data sheet for intensity meter with a radiometric sensor, page 1*

TECHNICAL DATA

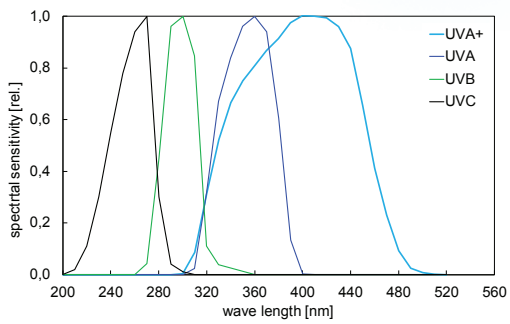

Spectral sensitivity UVA+, UVA, UVB and UVC sensors

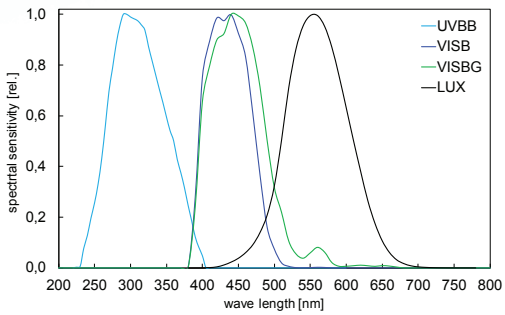

Spectral sensitivity UVBB, VISB, VISBG and VISL sensors

COMMON TECHNICAL DATA

Dimensions	Ø 40 mm, h 35 mm
Weight	150 g
Connecting cable	2 m
Operation temperature	0 to 40 °C
Storage temperature	-10 to 40 °C
Humidity	< 80% non-condensing

SENSOR SPECTRAL RANGES

UVC	200 - 280 nm
UVB	280 - 315 nm
UVA	315 - 380 nm
UVA+	330 - 455 nm
UVBB (broad-band)	230 - 400 nm
VISB	400 - 480 nm
VISBG	400 - 570 nm
LUX	380 - 780 nm, V(λ)

TECHNICAL DATA SENORS FOR RM-12

Operation voltage	+/- 5 V	
Signal voltage	0 - 2 V	
Sensor connector	M12 (5 pole)	
Measurement range	0 - 199 mW/cm²	
	0 - 1999 mW/cm²	(opt. -1)
	0 - 19,9 W/cm²	(opt. -2)
	0 - 19,9 mW/cm²	(opt. -3)

TECHNICAL DATA SENORS FOR RM-22

Operation voltage	+/- 3,3 V	
Signal voltage	0 - 2,5 V	
Sensor connectors	5 pole, pluggable	
Measurement range	0 - 200 mW/cm²	
	0 - 2000 mW/cm²	(opt. -1)
	0 - 20 W/cm²	(opt. -2)
	0 - 20 mW/cm²	(opt. -3)
	0 - 2 mW/cm²	(opt. -4)

PART NUMBERS

Radiometer RM-12	821200	**Radiometer RM-22**	822201
RM-12 sensor UVC	811010	**RM-22 sensor UVC**	812210
RM-12 sensor UVB	811020	**RM-22 sensor UVB**	812220
RM-12 sensor UVA	811030	**RM-22 sensor UVA**	812230
RM-12 sensor UVA+	811045	**RM-22 sensor UVA+**	812245
RM-12 sensor UVBB	811011	**RM-22 sensor UVBB**	812211
RM-12 sensor VISB	811040	**RM-22 sensor VISB**	812240
RM-12 sensor VISBG	811042	**RM-22 sensor VISBG**	812250
RM-12 sensor LUX	811061	**RM-22 sensor LUX**	812261

Opsytec Dr. Gröbel GmbH
Goethestr. 17, 76275 Ettlingen, Germany
Phone +49 - 7243 - 94 783 - 50
Fax +49 - 7243 - 94 783 - 65
www.uv-groebel.com
info@uv-groebel.com
certified according
DIN EN ISO 9001:2008

Figure C3 – *Data sheet for intensity meter with a radiometric sensor, page 2*